

MIE 415 Final Report

1411

Guide Dog Robot

Sponsored by: Dynamic and Autonomous Robotic Systems Lab, UMass Amherst

May 9th, 2025

Ken Suzuki	- Team Lead
Shaylyn Tavarez	- Analysis Lead
Salani Seneviratne	- Design Lead
Connor Delaney	- Fabrication Lead
Georges Chebly	- Controls/Electrical Lead
Peter White	- Evaluation Lead

Executive Summary

For the past three years, the Dynamic and Autonomous Robotic Systems (DARoS) Laboratory at UMass Amherst has been conducting studies on guide dog robots. However, the lab's current research platform, the commercially available UniTree Go1 quadruped robot, lacks the ability to climb stairs. Although the DARoS Lab has explored other commercial quadruped robots, none offer both good portability and stair-climbing capabilities at the same time. To address this gap, we present Vivo, a prototype quadruped robot that offers both stair-climbing capabilities and portability by having dimensions to allow it to be carried as a carry-on item on domestic flights. Vivo's legs are designed to closely mimic dog legs, which have long proven to be effective at stair climbing. The leg lengths are also optimized for stair climbing based on kinematic analysis. Additionally, the robot collapses to smaller than carry-on luggage dimensions, making it portable for daily use. This project has been deemed a success by the DARoS Lab and they will be continuing work on the prototype so that they can begin using it as their research platform.

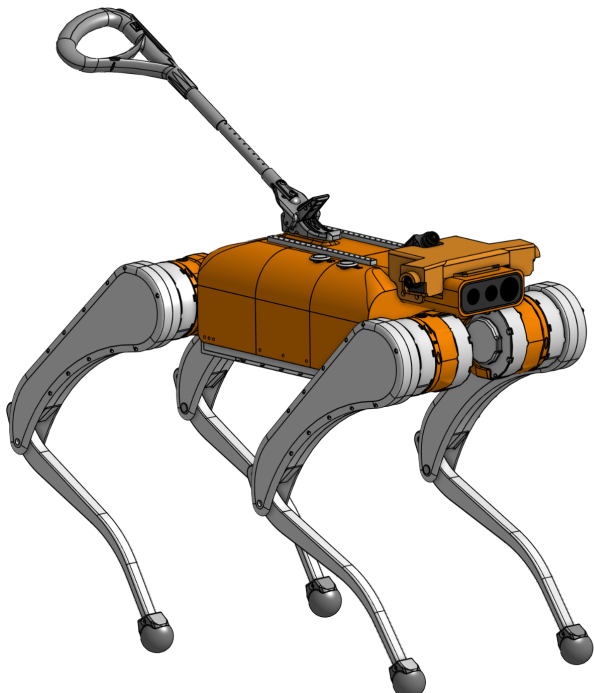


Figure 1. Current Design of Robot Guide Dog

Summary of Impact

The sponsors of this project sought to develop cutting-edge software for quadruped robots with the goal of creating a robot guide dog. While they have made progress towards achieving this goal, the hardware currently used for testing has proved to be the limiting factor in their research. For this reason our team has developed a prototype quadruped robot specifically designed to function as a guide dog. By addressing key issues faced by our sponsor such as stair climbing ability and portability we lay the groundwork for the lab's future research into robot guide dogs. This prototype will help establish the foundation for testing the concept of a specialized quadruped guide dog robot, effectively acting as a prototype for future versions. In the future this research will have been the first step towards the creation of a fully fledged robotic mobility aid for blind and low-vision (BLV) individuals.

Introduction and Objectives

Guide dogs are a popular aid for BLV individuals as they provide the user with greater mobility, confidence, and independence. However, guide dogs have several drawbacks that make them unsuitable for some people. A new guide dog generally requires two or more years of training before they are capable of working effectively, which can cost over \$40,000. Along with the upfront cost, dogs cost approximately \$1,200 yearly for general care ("How Much Does A Guide Dog Cost?"). Additionally, owning a dog comes with a lot of responsibility: they need consistent grooming, veterinary visits, and regular exercise. Finally, guide dogs typically work for only eight years, at which point the owner may have formed a strong bond, making it emotionally challenging to transition to a new dog (Hwang). In contrast, a robot guide dog offers a lower barrier of entry for BLV individuals seeking a reliable mobility aid. Unlike traditional guide dogs, a robot guide dog could be purchased off-the-shelf without a waitlist or need for extensive training. Both the upfront and annual cost of a robot guide dog would be cheaper than that of a traditional guide dog, providing a more affordable and sustainable solution. The DARoS lab has been using the Unitree Go 1 robot to explore computer vision applications for guide dog assistance, but significant hardware limitations— inability to reliably climb stairs, and a narrow field of view, restrict its usability for blind and low-vision (BLV) individuals. For this purpose, Vivo is designed to address all these issues and offer chances for better computer vision studies. The objective of our project is to design and fabricate the body and legs of a lightweight guide dog robot prototype capable of stair climbing while ensuring a compact body for portability and user-friendliness. This objective does not include the control and programming portion which will be done later by other lab members.

Related Works

The use of robotic systems as a mobility aid for BLV individuals have been investigated as early as 1976, starting with the MELDOG project, in the shape of a wheeled robot (Tachi). Since then, robotic mobility aids have taken the shape of drones (AI Zavier), smart canes (Slade), and advanced wheeled robots (Guerreiro).

In recent years, the locomotion of quadruped robots have become robust enough for commercial use and have become an increasingly popular solution to automating undesirable and dangerous tasks, such as safety inspection (“Industrial Inspection Solutions”). One of the underlying benefits of quadruped robots is their ability to traverse urban environments effectively, which makes them an attractive solution to mobility assistance for blind and low-vision individuals (Hwang).

Based on extensive qualitative research with guide dog users conducted by our sponsor, Hwang et. al, we aim to tackle the current limitations of portable quadruped robots for use as a mobility aid (Hwang). Currently, no commercially available quadruped robot matches the portability and stair-navigation abilities of a guide dog. Larger scale quadrupeds like the Boston Dynamics Spot robot and ANYbotics ANYmal C excel in stair-climbing, but their size makes them impractical for portable use. On the other hand, medium to small-scale robots such as the Unitree Go generation robots offer portability but lack the capability to traverse stairs of normal height (17.78 cm x 27.94 cm per ADA standards), which is required for a guide dog robot. This limitation creates a need for a compact quadruped robot that can traverse stairs (“Chapter 5: Stairways”).

Contributions of Each Team Member

Table 1. Team Member Contributions and Project Impact

Team Member/Role	Contributions
Ken Suzuki Team Lead	<ul style="list-style-type: none">• Created dynamic model of the robot using a URDF file• Communicated with team sponsors regarding progress, analysis, and design choices• Designed the final body• Conducted kinematic and inverse dynamics analysis of leg designs• Assisted with almost all aspects of the project
Shaylyn Tavarez Analysis Lead	<ul style="list-style-type: none">• Conducted structural by-hand analysis of robot legs• Led Presentation for faculty analysis review• Created shear force and moment diagrams for links• Determined key design constraints• Researched methods to perform structural analysis of robot• Assisted 3D printing leg prototype• Machined metal brackets on body• Assembled legs of robot• Assisted with the evaluation of stair climbing and size constraint
Salani Seneviratne Design Lead	<ul style="list-style-type: none">• Researched methods to perform structural analysis of robot• Performed structural by-hand analysis on the robot's leg designs under two conditions:<ul style="list-style-type: none">○ Equilibrium state○ Maximum dynamic load• Communicated with faculty for analysis review• Conducted calculations to find the impact forces on the robot• Presented the CDR and the final design and analysis presentation• Designed the pins for the 3D printed legs and assisted in designing other parts of the robot

	<ul style="list-style-type: none"> Helped with disassembling the Unitree Go1 to get the motors Helped with creating the BOM and ordering parts for the body Helped with assembling the legs of the robot and creating the body for the initial prototype Assisted in machining the brackets Assisted in assembling the legs and body of the final prototype Created the stand to keep the robot Worked on the stair testing of the robot
Connor Delaney Fabrication Lead	<ul style="list-style-type: none"> Performed FEA analysis of leg assembly Assisted team lead with statics analysis Assisted controls lead with interior configuration of robot Modified designs with the goal of improving manufacturability Disassembled Unitree Go1 Prepared and verified engineering drawings Fabricated frame for body of robot Assembled prototype robot Assisted in evaluation of prototype
Georges Chebly Controls/Electrical Lead	<ul style="list-style-type: none"> Optimized the body shape to make it manufacturable, compact, and able to fit within carry-on suitcase dimensions for final metal design Helped team lead in the inverse dynamics analysis Worked on the interior of the robot for original final metal design <ul style="list-style-type: none"> Decided on the electronics configuration Designed mounts for electronics (cameras, computers...) Set up hardware connection between motor and UpXtreme Established communication through RS485 Attempted to control the motor Helped with documentation through AOIs Assisted in assembling prototypes used for evaluation
Peter White Evaluation Lead	<ul style="list-style-type: none"> Helped with the preliminary research throughout the first semester including: material standards for Aluminum 6061-T6 and 1018 Carbon Steel, stair climbing and mobility analysis, and batteries Helped prepare and present AOIs, design presentations and

	<p>write reports</p> <ul style="list-style-type: none"> • Performed preliminary ANSYS analysis on the shank of the robot leg (later advanced and changed by someone else) • Helped with designing battery electronic mount and concepting/designing the new 3D-printed body design • Assisted with designing and manufacturing the several prototypes and final design • Performed a good portion of the additive manufacturing for the prototypes • Setup evaluation plan and helped execute it. • Helped with manufacturing, including creating a 9-stage program on the milling machine to cut out the arcs on the front and back motor brackets. • Designed the preliminary version of the front camera mount edited by Ken for the final design of the robot dog
--	--

Each member's contributions greatly impacted our ability to complete this project. Those who worked more heavily on the design allowed us to have a physical prototype by the end of the year, and those who worked more on analysis gave us the confidence the design would function as intended and avoid failure.

Functional Decomposition

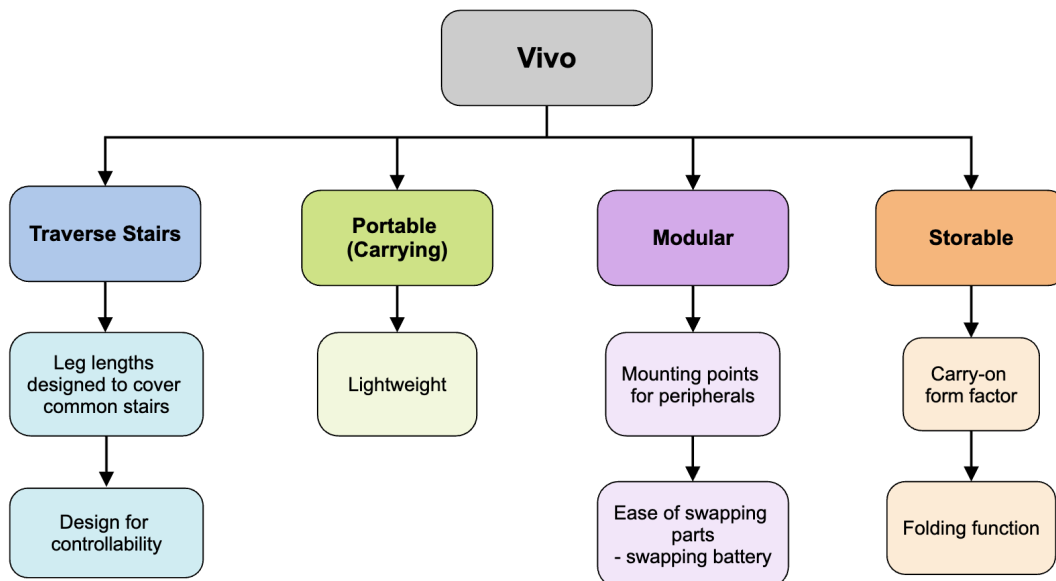


Figure 2. Functional Decomposition of Our Robot

In order to create a guide dog robot that meets the needs of a BLV user, the robot should be capable of performing four key functions, as illustrated in Fig. 2. First, the robot should be able to navigate urban terrain, which is crucial for guiding users during their travels. This includes overcoming common obstacles, such as stairs. To address this challenge the robot must have leg lengths and geometry capable of combating such obstacles and a design that is easy for controllability by using a ubiquitous 12 DOF, four legged system. Secondly, given that BLV users often rely on public transportation for daily travel, the robot must be lightweight and portable to facilitate easy handling. Lastly, to ensure convenience and usability, the robot should conform to standard carry-on suitcase dimensions, allowing it to be easily stored when not in use, and be modular. The robot should have the capability of allowing the user to easily swap batteries when they are close to failure, and be set up to allow the Sponsor to make quick modifications of the inner components for future iterations. Functions related to software were not included in the functional decomposition due to it being outside the scope of our project.

Engineering Standards and Patents

Material Standards

The final design analysis was done using two material standards. The majority of the robot is made up of aluminum 6061-T6 and the transmission link is made of 1018 carbon steel. The ASTM standard specification for aluminum 6061-T6 material strength was used in analysis and the AISI/SAE 1018 carbon steel specification was used in analysis for steel components. The ASTM standard specifies aluminum 6061-T6 to have an ultimate tensile strength (UTS) of 260 MPa and yield strength (YS) of 240 MPa. The AISI/SAE mechanical properties for 1018 carbon steel are rated at a UTS of 440 MPa and a YS of 370 MPa. These standards help to improve the quality of our design by providing reliable material properties for analysis.

Robotics Standards

ISO 13482 sets guidelines for the safety of personal care robots with respect to electrical, mechanical, and software. These guidelines have helped pave the design process to ensure safety and reliability. Following the guidelines for robot design, hard stop limits at each joint for singularity protection must be incorporated. Joints shall not be capable of crushing any body parts. User interface guidelines highlight the need for status indication and avoidance of sharp edges and points on the robot.

Manufacturing Standards

ISO 286 provides guidelines for tolerancing components in 2D drawings. As our sponsor intends to fund the manufacturing of robot parts through an overseas contract manufacturer, this standard will serve as the basis for communicating the geometry and tolerances of our components to them. This will be crucial for reliable operation of the legs.

Stair Standards

ADA § 504 & IRC § R311.7 outline the requirements for both residential and commercial staircases, including the maximum and minimum lengths for stair steps (“Chapter 5: Stairways”). Designing our robot to be capable of climbing stairs means it must be able to climb the tallest stairs specified by these codes to ensure compliance with standards. According to the International Code Council, the maximum step height is twenty centimeters and the minimum step length is twenty-five centimeters (International Residential Code). In contrast, the Americans with Disabilities Act defines the maximum step height as eighteen centimeters and the minimum step length as twenty-eight centimeters.

Patents

Patents were used to gain knowledge of the current competition and to obtain inspiration for our robot design. Boston Dynamics’ Spot robot features an elbow joint actuated by a ball screw mechanism acting as a prismatic joint, which differs from belt driven or parallel link driven mechanisms that are popular in small scale quadruped robots (Potter). Although this mechanism is complex compared to other elbow actuation methods, it is highly efficient at transmitting force. The ANYmal C robot developed by ANYbotics features a limb between its top and bottom links, with a built-in series elastic actuator that introduces passive compliance into the joint, which is a feature not present in traditional planetary gear box reduced brushless DC motors (Scafato).

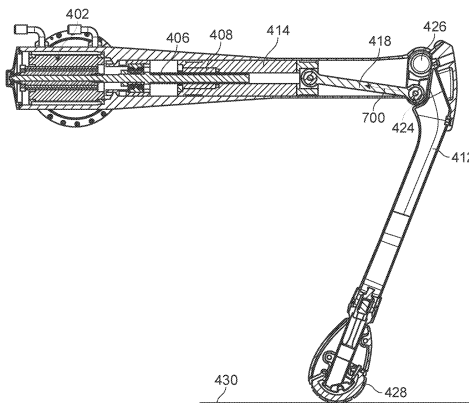


Figure 3. Leg design of Boston Dynamics’ Spot robot (Potter).

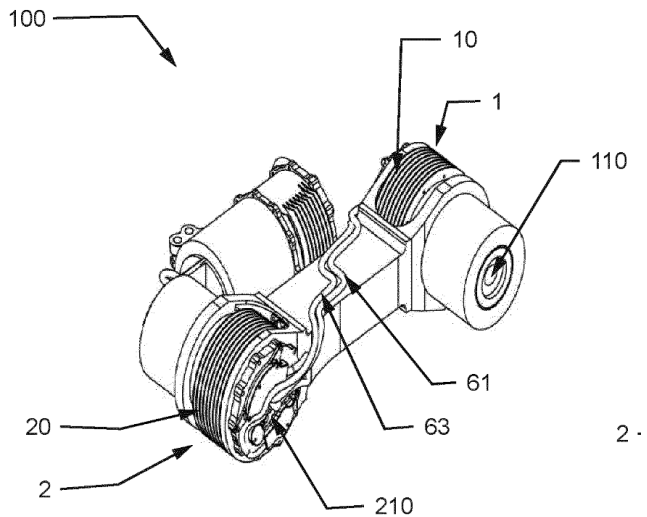


Figure 4. Limb design with incorporated series elastic actuators, developed by ANYbotics (Scafato).

Specifications

Table 2. Customer Requirements

Requirement	Weight
Storability/Small Size	3
Portability	2
Cost	1
Hardware For Stair Climbing	4

*(Level of importance: 1 (Least) → 4 (Most))

The customer presented an initial list of requirements at the start of the semester which was refined through further communications. The customer expressed that the final product must meet two major requirements: hardware capable of stair climbing, and a portable form factor. From this, the team made these requirements of utmost importance as seen in Table 2. The requirement of a portable form factor is split into storability and portability since the customer emphasized that the quadruped should be lightweight, and be able to fold into airplane carry-on luggage size. Cost was put low on the list originally since the customer was open to financing the final product if the

requirements were met, but the budget as with any project was still a consideration. Later in the year the lab had more financial constraints and was not able to get an NIH grant for this project due to federal funding pauses. Due to this, cost was highly considered when creating the final design presented in Fig. 1, though the other requirements were still of utmost importance.

Table 3. Target Engineering Specifications

	Reachable Workspace (rise/go) [m/m]	Mass [kg]	Storage Volume [m³]
Ideal Values	0.20/0.25	≤ 21.5	< 0.45
Marginal Values	0.18/0.28	25	0.45

The engineering requirement specifications are presented in Table 3. The storage volume criterion was determined by using the average maximum collapsible carry-on volume in the United States of $55.88 \times 35.56 \times 22.86 \text{ cm}^3$. Achieving this form factor is necessary, but any value below this is ideal (Norcross). An ideal weight of 21.5 kg was imposed based on the weight of the Unitree Aliengo robot, which is slightly larger in size than our maximum allowable dimensions. The weight was also chosen to prevent strain on the user or carrier when the dog has to be lifted. The dog's ability to climb stairs is based on research out of the Italian Institute of Technology, which found that quadrupeds that have successful foot candidate positions that cover at least 20% of the "Go surface" climb stairs effectively. In accordance with the previously discussed IRC § R311.7 and ADA § 504 standards, we determined the ideal and marginal rise/go values that the robot must be able to climb. The ideal value was established using the higher rise/go ratio from the two standards, while the marginal value was based on the lower ratio. See Fig. 5 for go and rise definitions.

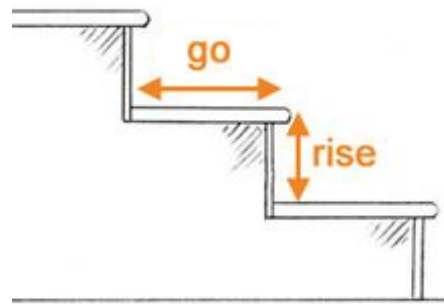


Figure 5. Staircase diagram defining rise and go.

Similar products were compared to further determine the necessities of each customer requirement. As seen in Table 4, our product has the best overall combination of the customer requirements compared to other options on the market. The UniTree Go1, a small-scale quadruped robot, excels in terms of storability and portability; however, it is unable to climb standard stairs effectively. The UniTree Aliengo and Boston Dynamics Spot are both larger scale quadruped robots. This allows them to score well in hardware for stair climbing due to larger legs. However, since they are larger robots they fail to meet storability and portability requirements and are more expensive.

Table 4. Customer Requirements- Our Design Versus Competition (1 (Worst), 5 (Best))

	Our Product	Boston Dynamics Spot	UniTree Go1	UniTree Aliengo
Storability	5	0	5	1
Portability	5	1	5	4
Hardware for Stair Climbing	4	5	2	4
Cost	4	1	5	2

Design Selection and Solution

Leg Design

The initial leg design consisted of the conventional, simpler two-link leg (Fig. 6) for design simplicity. However, recent works in the field of control aware robot design suggest that bio-inspired leg designs are more dynamically efficient, leading to less power consumption (De Vicenti; Seok). Thus, our second design iteration utilizes a dog-inspired leg design to maximize system efficiency. We modeled our leg designs similar to that of a golden retriever, which is a common dog breed for guide dogs (Durant; Piper). As illustrated in Fig. 7a, our second design concept featured different legs for the front and hind legs. The front leg featured a two-link, two-degree-of-freedom leg, while the hind leg featured a three-link, two-degree-of-freedom leg. However, due to safety concerns with the linkage having the potential to pinch the user, as well as design complexities that hinder ease of assembly, for our final design, we went back to utilizing the simpler, two-link leg design for all legs.

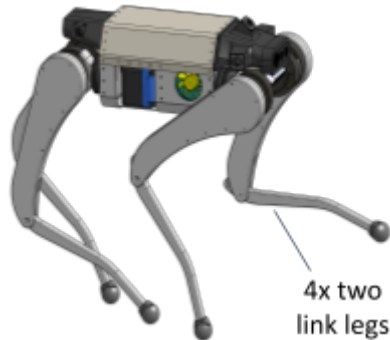


Figure 6. First concept of the robot with four two link legs.

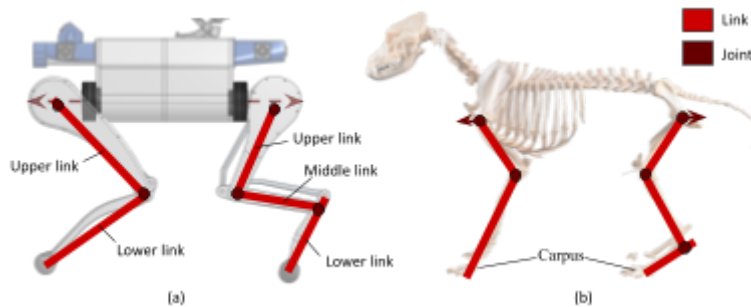


Figure 7. Link configuration of second bio-inspired design iteration. (a) our robot's legs to (b) golden retriever legs (Museum of Veterinary Anatomy FMVZ USP).

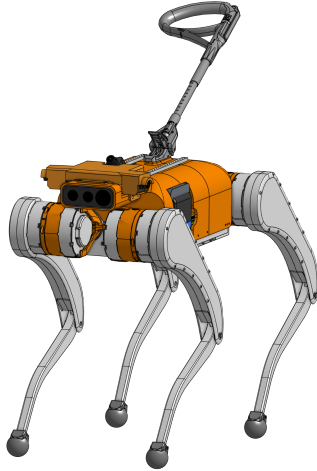


Figure 8. Final leg configuration

Actuation Mechanisms

The leg actuation method was important to decide early on in order to guide our leg design and motor selection. Three systems were considered: transmission links, timing belts, and driving links directly with the motors. Out of these three, the option to drive the links directly with the motor was discarded. While this system would be the simplest to implement mechanically, it has several drawbacks. Most notably, placing a motor at each joint would increase the inertia of each leg from the added weight. This results in legs that weigh more, take up more space, consume more power, and cost more. For these reasons driving links directly was discarded.

Timing belts to actuate the legs were the second option considered (Fig. 9b). Compared to directly attaching motors in each joint, timing belts offer several advantages. The moment of inertia in each leg decreases with a timing belt as the weight of the motor is moved toward the body of the robot. However, timing belts are hindered by slippage and experience decreased durability when improperly tensioned. If a timing belt is not properly tensioned during use, these issues build up over time leading to premature failure (Layosa). It would be difficult for BLV individuals to perform this maintenance on their own, which motivated the decision to use transmission links (Fig. 9a).

Transmission links have several benefits for a quadruped robot of our size that make them the ideal choice. Similar to timing belts, they allow all the motors in the robot to be located in the body, reducing the moment of inertia in the leg. Transmission links are also very durable which help reduce potential maintenance required in other systems. When the transmission link mechanism is configured in a redundantly actuated, parallel configuration, the elbow joint rotates at the same angle as the

motor output angle. The only drawback of transmission links is the potential of backlash in the mechanism, which may cause inaccuracies in the kinematic model of the leg and cause noise during locomotion. However this can be mitigated with precise manufacturing, to keep the relative location of the pins as tightly configured as possible. With minimal backlash, the control of the robot is almost as precise as the control of the motor can be. For these reasons, the transmission link was the selected actuation method.

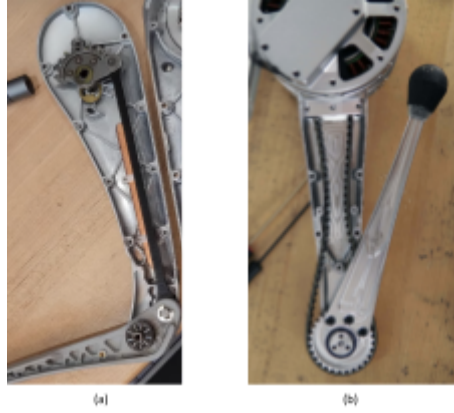


Figure 9. Elbow actuation mechanisms considered.
 (a) Transmission link (RegulusRemains) (b) timing belt (Katz).

Motor Selection

Motors were selected based on the dynamic requirements of the robot. Additionally, using lower-power motors was held paramount to prolong the robot's battery life. Since the robot is not intended to perform highly dynamic motions, the motor torque should be able to handle walking and stair climbing and nothing more. Brushless DC motors were selected due to their higher efficiency, lower operating noise, and higher angular velocity compared to other types of motors. They are also the most popular type of actuator used in legged robots today. The selected motors are the Unitree GO-M8610 motors. Through inverse dynamics calculations, the combined effort of the selected motors are able to withstand approximately twice the robot's estimated weight while standing (see "Dynamics Analysis" subsection).

Body Design

The body of the robot is designed to contain all the electronic components necessary to control the robot. The design has been set to have the strength to sustain loads from the legs and bear the weight of the inner components. In order to do this the outer body was originally planned to be

constructed using aluminum sheets and plates for their high thermal conductivity and lower cost. Compared to other types of materials such as injection molded plastic, aluminum does not require the creation of a custom mold, which would be costly. While 3D printing the body (Fig. 10a) is another option, it was thought to compromise the strength of the structure due to the anisotropic properties of additively manufactured parts. In addition, the thermal conductivity of a plastic is lower relative to most metals, which may compromise the heat dissipation needed because of the electronics. Aluminum was chosen over a metal like copper because of its high strength while also maintaining good thermal conductivity (“Copper, Cu; Annealed”). The electronics mounts inside the body were placed symmetrically along the robot’s sagittal plane to keep the center of mass as close to the center as possible, ensuring equal weight distribution across the interior. Ample space in the sides of the interior provided room for cabling. Additionally, the robot’s belly thickness (i.e. the vertical distance between the hip axis and the lower body) was minimized to maintain a higher clearance from the ground during stair climbing. Fig. 10b shows an aluminum plate positioned in the middle, connecting the sheet metal components. However, it was found that including this plate would complicate the assembly process due to a large number of components required for assembly. To simplify the assembly, the next iteration of the body structure (Fig. 10c) was composed of four aluminum components (two plates, two metal sheets). Lastly, the computers were positioned distant from each other to disperse their generated heat to a wider area in the body interior to prevent the buildup of high temperatures.

This was originally the choice for the final body design, however due to new found funding constraints with the lab, the legs could be manufactured, but not the aluminum body. The body was then redesigned (Fig. 10d). All body designs were developed while considering the robot’s stair-climbing capabilities and fabrication efficiency.



Figure 10. Body design progression. (a) 3D printed design. (b) Four-piece sheet metal design. (c) Two-piece sheet metal design (d) Metal frame with 3D printed covers

For the final iteration of the body design (Fig. 10d), cost efficiency was key in order to be able to afford manufacturing (see “Cost Efficiency” section). Utilizing metal frame derived from custom

off-the-shelf parts and 3D printed components, the metal frame acts as reinforcement to sustain reaction forces from the legs, while the 3D printed components act as mounts for electronics components. The ability to 3D print the frame serves as the connection point for the cover and base of the robot dog, and allows for greater modularity. The base (bottom center in Fig. 10d) of the robot is an acrylic plate which serves a mounting point for electronics. Acrylic was chosen for its cost effectiveness and adequate strength, given the minimal weight of the electronics. Acrylic is relatively low cost and has a higher yield strength than comparable plastics such as polycarbonate. The electronic mounts have been spread out to balance the weight in the robot and to allow for ample room for the cords necessary for the power electronics setup (more details in “Detailed Design” section).

Power Electronics

To reliably power the robot’s onboard computers and motors, power electronics were configured specifically for the robot. The robot’s power electronics take into account the following principles: reliability, safety, and failsafe mechanisms. The power electronics setup consists of several anti-spark switches and built in short circuit protection modules that act as RC filters. These components work together to act as a safety net to prevent excessive current draw, which may cause irreversible damage to the robot’s onboard electronics. As shown in Fig. 11, the computer and motor power electronics are isolated via anti spark switches, and a buck converter that converts the battery’s 24 V down to provide the computer’s required 12 V of power. A motor power distribution board helps distribute the power to the motors.

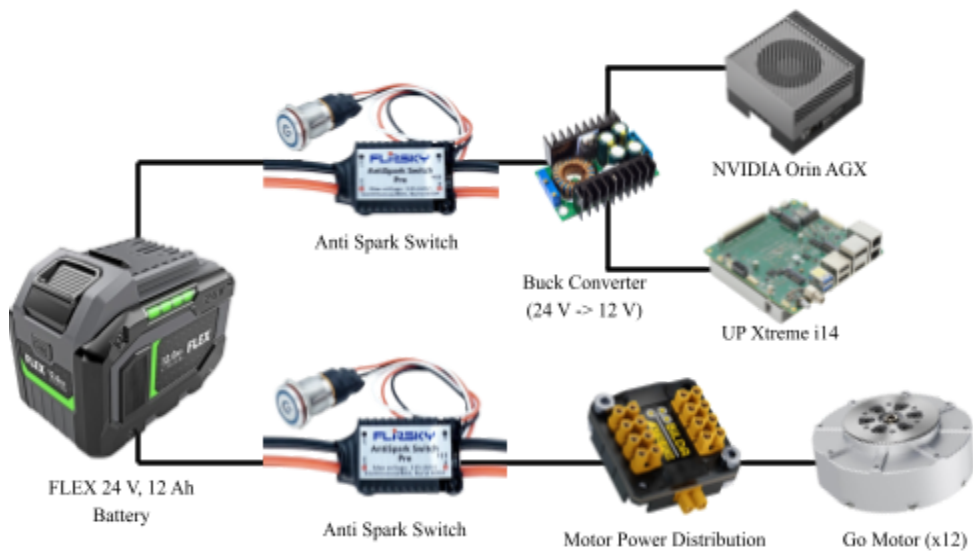


Figure 11. Diagram of power electronics setup.

Detailed Design

Legs

Each leg has 3 degrees of freedom to accommodate our customer's locomotion controllers, with each degree of freedom being depicted by the red joint axes shown in Fig. 12.

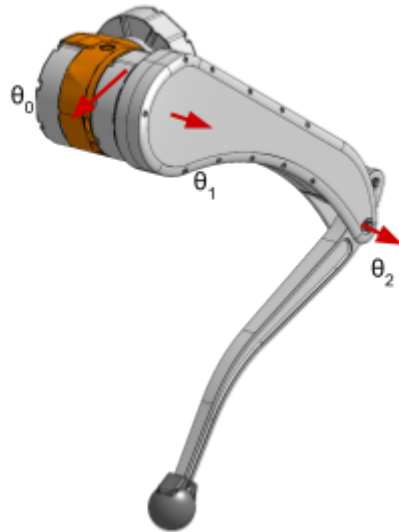


Figure 12. Joint configuration of front and hind legs. Both the front and hind legs have three degrees of freedom, where the middle link and lower link of the hind leg are coupled.

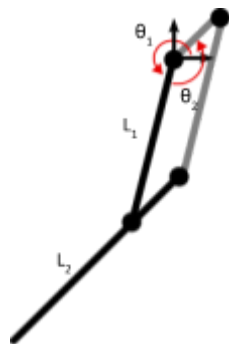


Figure 13. 2D kinematics diagram with hip DoF neglected.

The leg lengths were optimized through a stair-climbing evaluation method developed by Barasuol (Barasuol). The details of this analysis will be covered in the "Detailed Engineering Analysis" section. Using the stair climbing analysis, we aimed to make the body height as short as possible to promote a lower center of gravity for stable walking, while maintaining a > 30% coverage of the stair

surface, which exceeds the 20% coverage requirement for stair climbing as noted by Barasuol et al. (Barasuol).

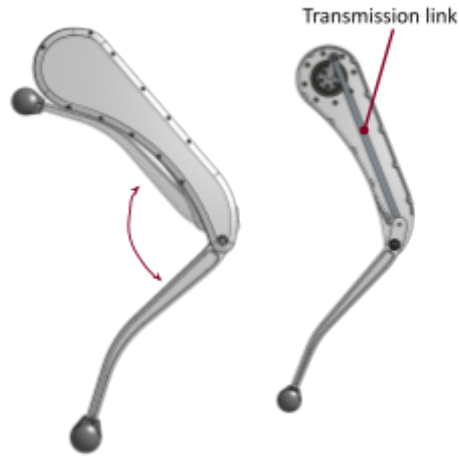


Figure 14. Leg Final Design and Actuation

For the redundant parallel transmission mechanism, a combination of radial ball bearings and steel pins were utilized at each revolute joint, which is a common design choice for many quadruped robots (Katz). Radial ball bearings were selected due to the absence of axial loads during locomotion, with the added advantage of ball bearings having overall lower friction, reducing energy losses. The internal transmission links are modeled with AISI 1018 steel to ensure a compact frontal profile of the leg, while the linkages themselves are modeled with Aluminum 6061 to minimize the leg weight while maximizing manufacturability. Lastly, the point foot is modeled as thermoplastic polyurethane (TPU), which can be 3D printed. This elastomer was selected as the foot material because it provides an ideal coefficient of friction, and its 3D printed structure allows easy access for manufacturing.

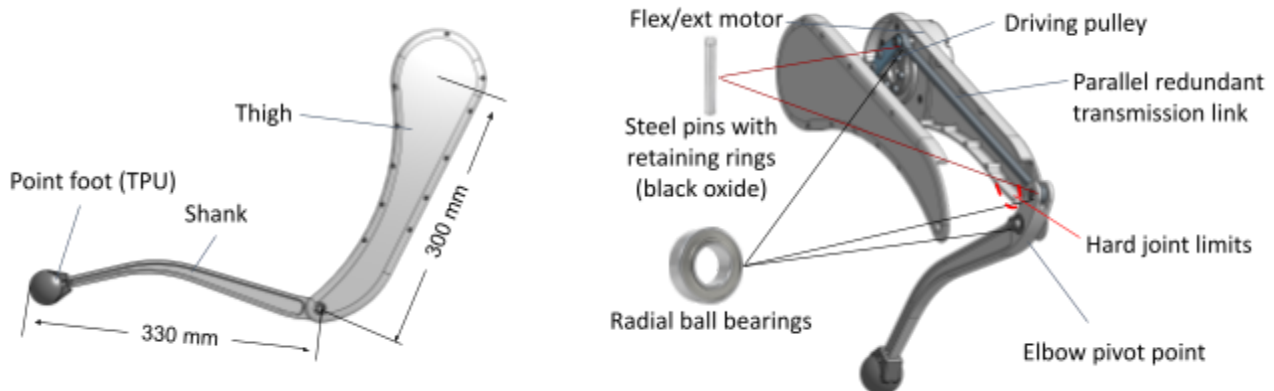


Figure 15. (Left) Leg size and design features. (Right) Internal Leg Mechanism. Transmission links (grey) are made of steel, and the linkages (white) are made with aluminum.

The cross sections for the leg designs were selected based on weight and manufacturability. It is to be noted that we plan on getting the components milled via a contract manufacturer. Aluminum 6061 T6 was the selected material for the leg structure, as it provides low cost, ease of manufacturing, and an optimal strength to weight ratio compared to other materials. Based on the statics analysis presented in the “Detailed Engineering Analysis” section, the I-beam and square profiles were found to be the most feasible to be manufactured via milling. In the end, the square profiles were selected for their exceptional manufacturability and largest stiffness. As a safety precaution, and a suggestion from our TA during the first semester, an impact force analysis was conducted to ensure that the robot is able to withstand abrupt drops (see “Impact Force Calculation”). A more detailed exploded view of the leg is shown in Fig. 16.

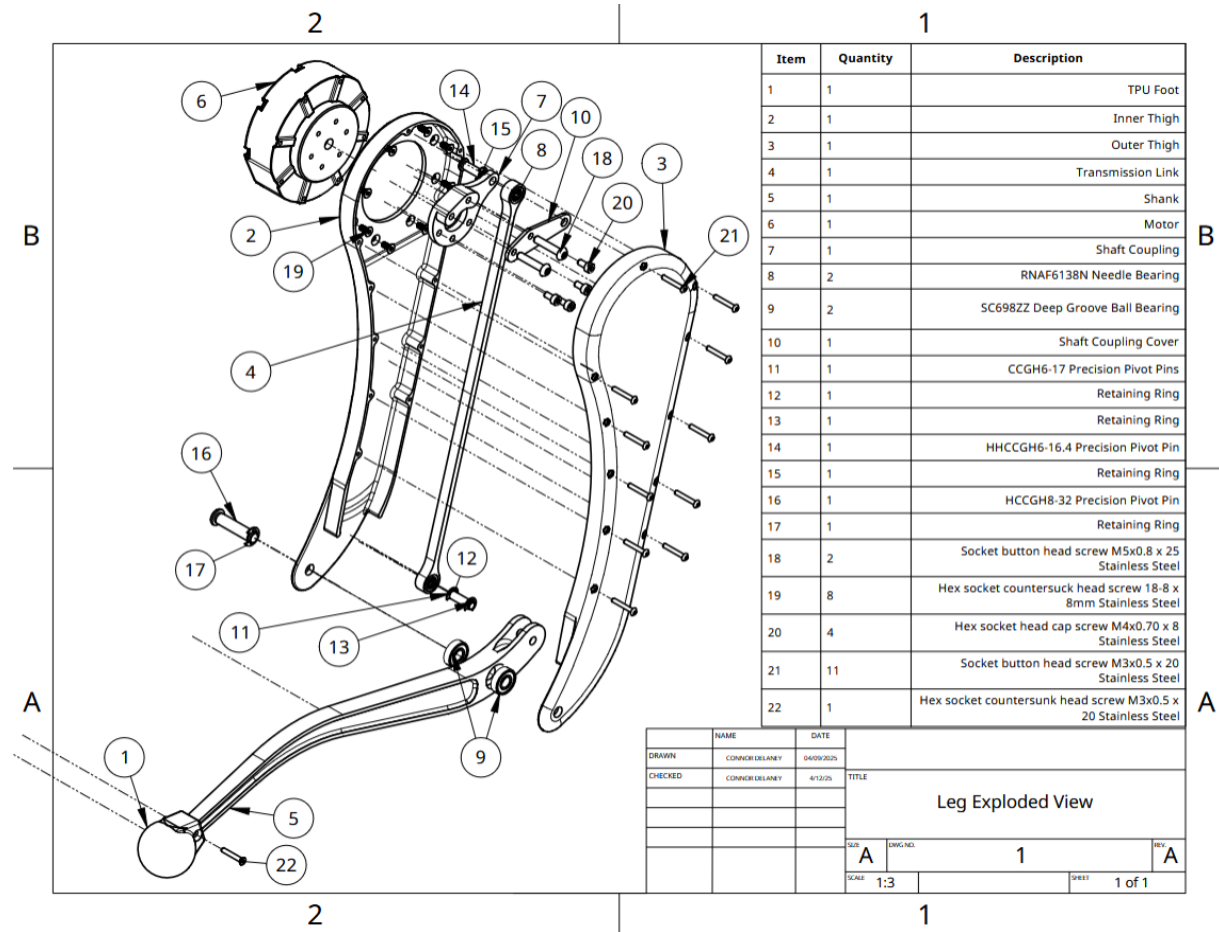


Figure 16. Exploded View of Leg Design

Body

The body design underwent several iterations to get to the final version. Aluminum was chosen originally as the primary material due to its combination of relatively high strength, good workability, and excellent corrosion resistance and has continued to be a centerpiece in the new design. The final dimensions of the body provide ample space to house all the electronics while maintaining a compact form factor that fits neatly into a carry-on suitcase dimensions.

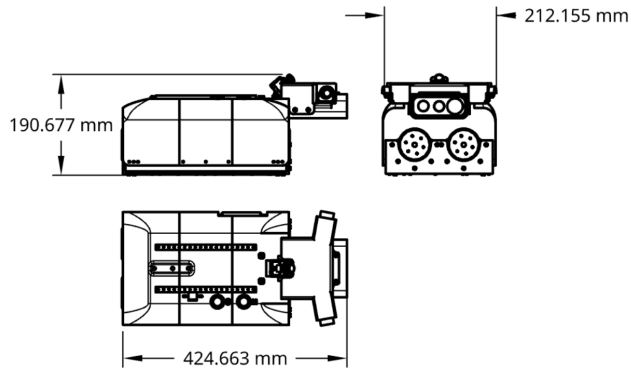


Figure 17. Final Dimensions of Body

The final body is constructed using two larger aluminum brackets positioned at the front and back of the robot and two smaller aluminum brackets along the lengths (Fig. 18). The bottom plate (plexiglass) and frame brackets are encased by 3D printed covers that cover the internal electronics, and provide mounting points for the harness handle, power buttons, and computer I/O. The reinforcing metal bars connecting the covers are lightweight and small to prevent any deflection and are used to maintain better structural stability for the covers. This design ensures a strong and durable structure while optimizing interior space for electronics placement. The components inside are arranged to prevent overheating, with the two mounted computers having fans that point in opposite directions. The power button cord is long, and will not prevent the cover from being easily removable. The cover is made of polylactic acid (PLA) and split into three parts connected with reinforcing metal bars. This cover was designed to be easily removable by removing screws along the length of the dog that connect the cover to the frame for future changes by the lab. While 3D-printing the body had concerns earlier on, that was in relation to the entire body being 3D-printed. For this body design, only the cover is made of PLA while the frame is made of aluminum structural stability.

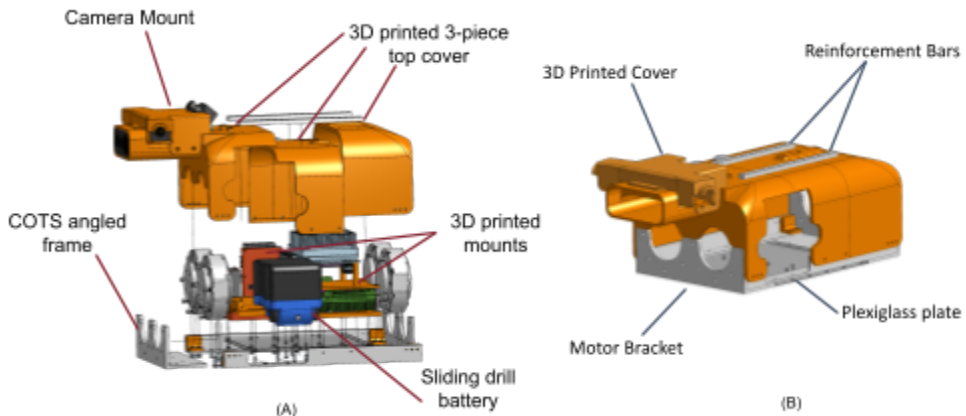


Figure 18. Internal layout of final design

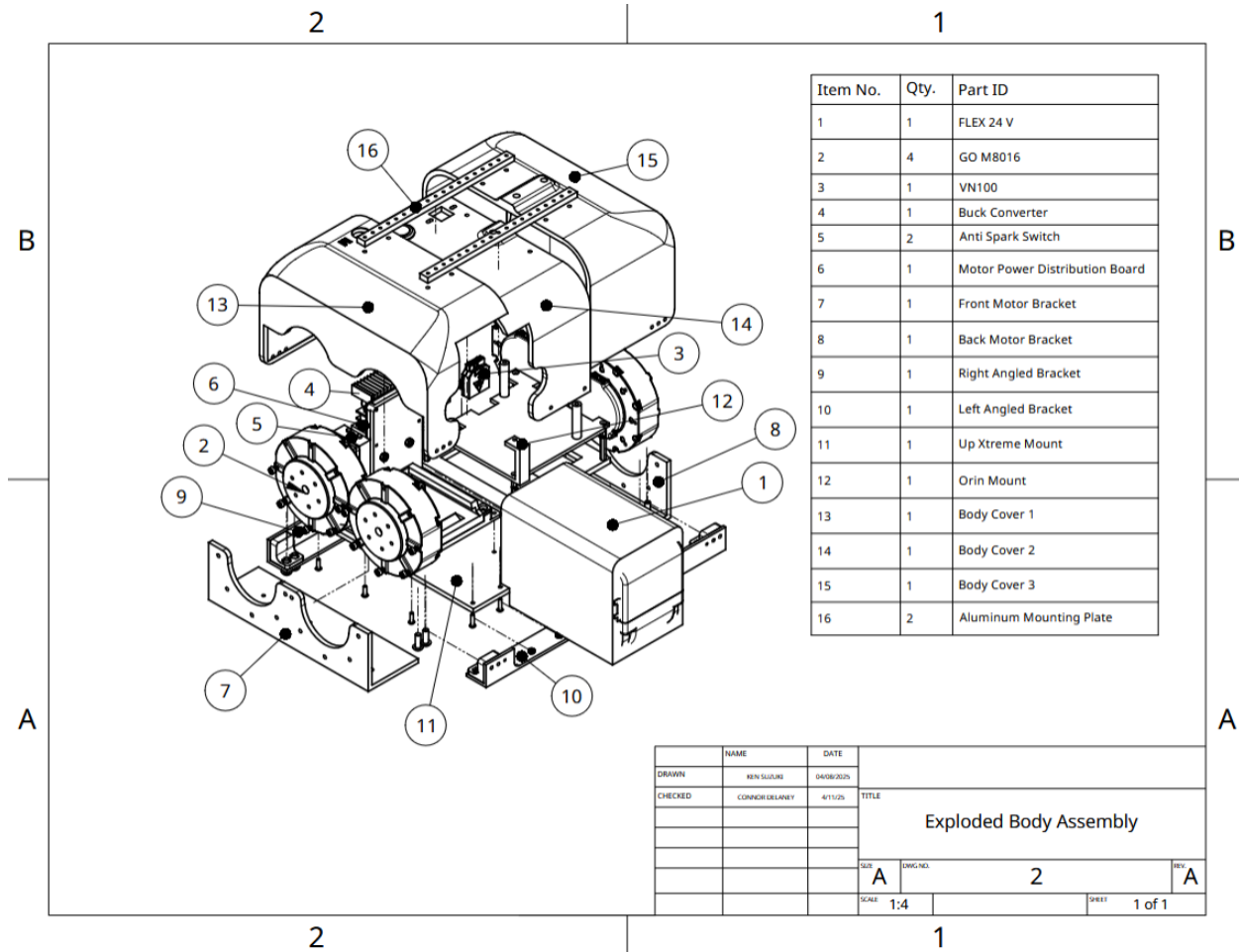


Figure 19. Exploded View of Final Body

The aluminum brackets were selected based on already available materials in our sponsor's workshop to keep costs low. Since our sponsor already had 3/16" inch thickness stock aluminum angles, we elected to utilize them. After the off the shelf components of the body were selected and a concept design was created, a by-hand structural analysis of the metal frame was conducted to validate its durability (see "Deflection and Strength Analysis of the Body" section). A more detailed exploded view of the body is shown in Fig. 19.

The final camera mount design is integrated into the front cover piece of the body as seen in the final mount design shown in Fig. 20. This design required multiple iterations to make sure it met the requirements of the sponsor for the front camera setup (10 degrees for the two side ZED cameras from the vertical (going clockwise) on the left and right and 40 degrees upward for back ZED camera), while also keeping the cameras safe and allowing for quick removal or modification. The design also had to allow ample room for the ZED camera wires to bend and work their way into the body for

connection with the computers. This was the motivator for having the mount integrated into the front cover piece. The initial design had a major flaw where the back ZED camera would not be able to be removed after installation. A larger plate was added afterwards to account for this, but the design was not easily modifiable or robust. Instead of having the “walls” surrounding the cameras as part of the base, a separate cover was made to serve this function instead which could simply be screwed in on top of the base.

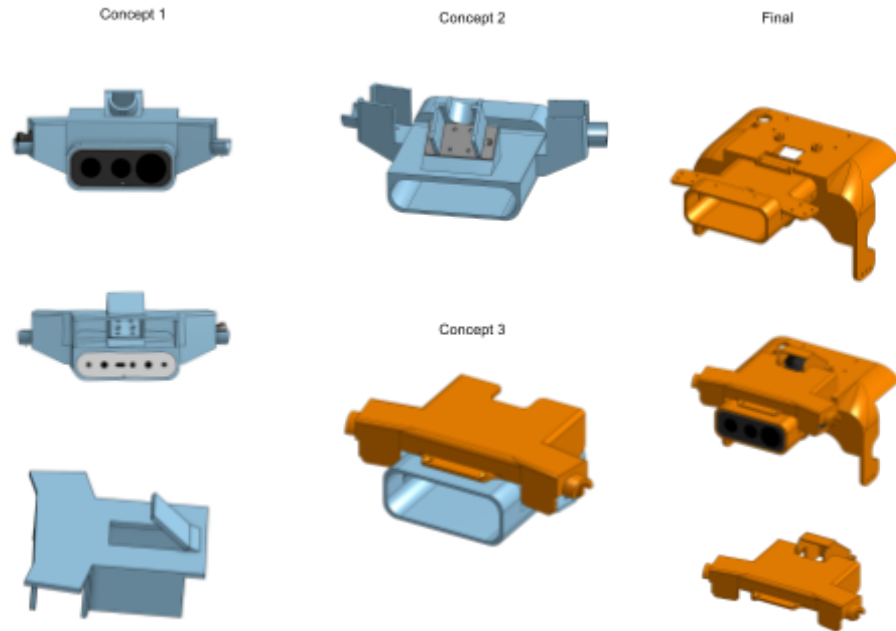


Figure 20. Camera Mount Design Iterations

During prototyping and testing (see evaluation section) it was found that the motor apparatus (Fig. 21) was not accounted for in the length of the body, making the robot too long when the legs and outer motors were attached. After this the maximum distance between the motors on the brackets was determined and adjusted for the final design (Figure 19).

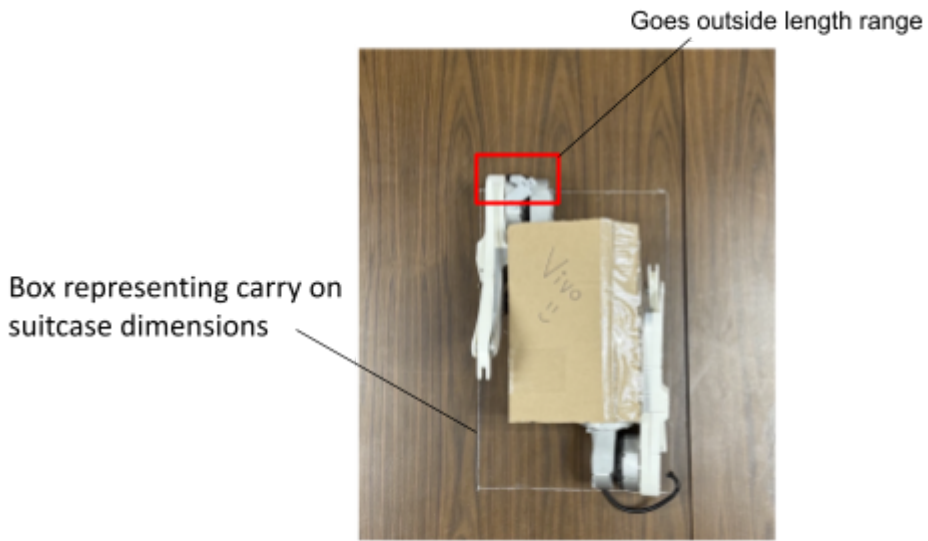


Figure 21. Motor Apparatus Problem

Throughout the design process, manufacturability was a key consideration. Components were designed with practical production methods in mind. Our body consists solely of off the shelf and 3D printed components, easing sourcing of the parts and lowering costs. The holes and extruded cuts on the metal components all are designed to be processed using a manual milling machine. Further manufacturing drawings of the design are shown in Appendix E.

Feedback From Sponsors and Mentors

To validate our design and analysis, we consulted with four faculty members from the Department of Mechanical and Industrial Engineering at UMass Amherst. During our design stage, Professor Frank Sup recommended exploring bio-inspired leg designs and different link lengths to enhance locomotion efficiency. Professor Govind Srimathveeravalli advised against using FEA for structural validation and encouraged us to rely on by-hand statics calculations, given the material strength of aluminum and steel under simplified beam assumptions. While we followed this guidance and completed all initial analysis by hand, we subsequently used ANSYS to validate our results. We also met with Professor Yubing Sun, who helped us verify our statics analysis. Additionally, we consulted our sponsor, the Dynamic and Autonomous Robotic Systems Lab, to confirm our kinematics, dynamics models, and our final design. Bi-weekly meetings were held with the sponsor to go over progress and design considerations. For our final faculty review, we met with Professor Tingyi Leo Liu, who reviewed our basic analysis, FEA results, and advanced dynamic simulations. He emphasized the need to better distinguish our team's contributions from the work of the sponsor's PhD students and

pointed out that we should accelerate our manufacturing and testing procedures. He also suggested strategies to improve our project delivery, particularly in how we present our work during the final showcase, such as putting side by side comparisons of the hand calculations with results from ANSYS.

Cost Efficiency

3D printing technology will be utilized for the camera mounts, point feet, internal electronics mounts, and body covers for its ease of manufacturing and low cost. The use of TPU for the point feet and covers allows us to 3D print in house, cutting costs. The electronic mounts, covers for the body, and the camera mounts (part of body covers) will be 3D printed from PLA due to its ease of access and the ability to more easily edit small features of the design in future iterations. A down selection process was used when determining the manufacturing method for the body and the legs to minimize cost while ensuring quality and structural integrity. Ultimately through this process sheet metal was chosen originally as the main material for the body since it is less expensive to manufacture than most other similar metals. However this was not enough of a cost saving measure after budget cuts during the second semester, leading us to our final body design as discussed previously.

Detailed Engineering Analysis (Selected Design)

Structural Analysis of Legs:

When performing dynamic motions like stair climbing the front and hind legs will experience higher loads than when in a static position. Part of ensuring the quadroped's capability of climbing stairs is ensuring the links which make up the legs can withstand the different loads that come with walking. Free-body diagrams were created for each link within the front and hind legs. Fig. 17 demonstrates the free body diagrams for the linkages of the front leg. Similar free body diagrams were found for all linkages.

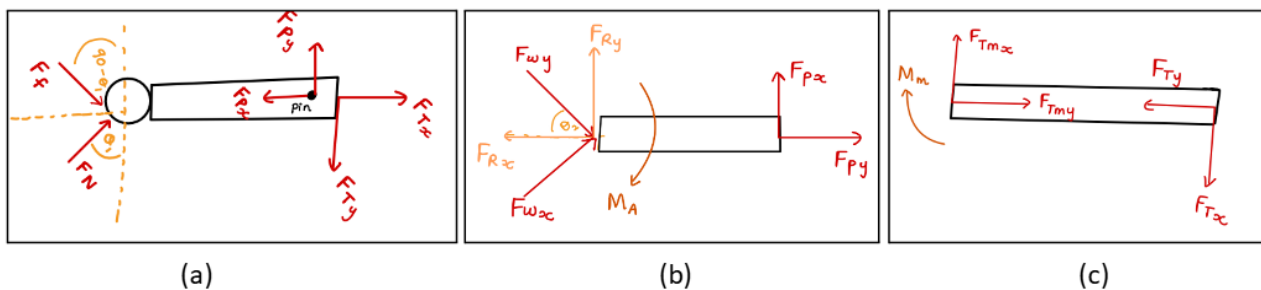


Figure 22. Free Body Diagrams for the front leg: (a) Lower Link (b) Upper Link (c) Transmission Link

In order to create these free body diagrams the complexity of the outer shape of the linkages was ignored since it does not impact the linkages strength against normal forces. The system was assumed to be in equilibrium and the force equations were found by assuming,

$$\sum M = 0 \quad \sum F = 0, \quad (1)$$

with M being the moment about any point and F being the forces. The MIT Cheetah 3 has a similar leg design with a similar weight constraint and was found to have a maximum dynamic load of two times the robot's weight (Bledt, 2019). With the equations being found in equilibrium a maximum dynamic load of two times the robot's weight was incorporated into the force equations to account for the force during dynamic motion. The linkages were assumed to be simple beams as there is no torsional force acting on any of the beams and all forces and moments were assumed as point loads. Shear-force and bending moment diagrams were created to determine the internal forces and moments within the linkages.

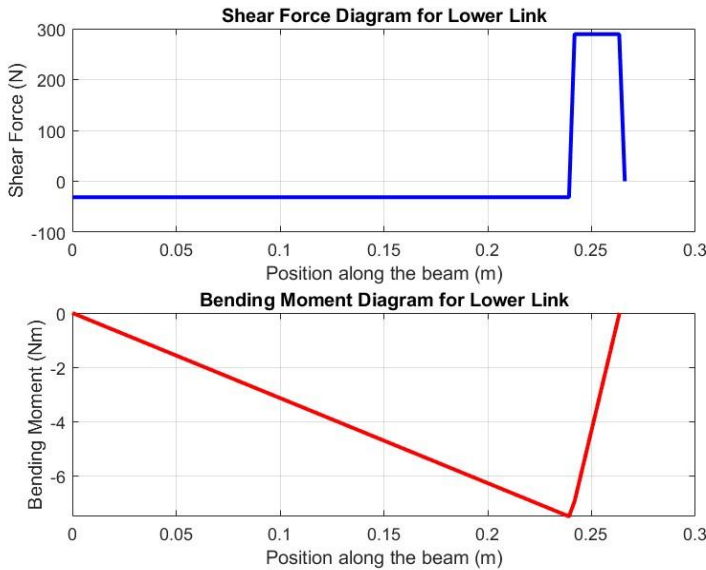


Figure 23. Shear force and bending moment diagrams for the front lower link

Fig. 23 demonstrates the shear-force and bending moment diagram for the lower link of the leg. Similar diagrams were found for all the links. When the shear-force and bending moment diagrams both go back to zero it indicates the assumptions made and the force equations found are accurate. Using the internal moment and forces of the linkages the design constraints for the cross-section were found by using the section modulus.

The section modulus stems from the cross section of a beam and is defined by,

$$S = \frac{I_z}{c}, \quad (2)$$

where I_z is the moment of inertia and c is the distance between where the maximum stress occurs and the neutral axis. The section modulus can be utilized as a constraint when creating the cross-sectional area of the link.

The section modulus originates from:

$$\sigma_{max} = \frac{(M_{max} \times c)}{I_z}, \quad (3)$$

where σ_{max} is the maximum allowable stress, and M_{max} is the maximum bending moment. Using the bending moment diagrams the maximum moment was found while the maximum allowable stress was found by utilizing,

$$FOS = \frac{\sigma_{yield}}{\sigma_{max}} \quad (4)$$

where FOS is the the desired factor of safety and σ_{yield} is the yield strength of the l. A factor of safety of 10 was used to deter high stresses from being applied to the links. The transmission links are made of Carbon Steel 1018 while the rest of the links are made of Aluminum 6061-T6. By simplifying equation 3 the section modulus can be found using

$$S = \frac{I_z}{c} = \frac{M_{max}}{\sigma_{max}}. \quad (5)$$

Table 5 contains the constraints for all links in both the front and hind leg in order to withstand the stresses from the maximum dynamic load.

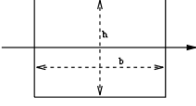
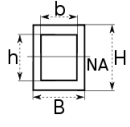
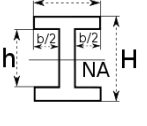
Table 5. Design constraint for section modulus of all legs

Front Leg	
Link:	Section Modulus:
Lower	$S \geq 0.31 \text{ mm}^3$
Upper	$S \geq 3.47 \text{ mm}^3$

Front Leg	
Transmission	$S \geq 2.38 \text{ mm}^3$
~	~

Using Table 6 a cross-section can be chosen that conforms with the design constraint laid out in Table 5.

Table 6. Equations to calculate section modulus for different cross sections

Shape of cross section	Section modulus equation
Rectangle 	$S = \frac{bh^2}{6}$
Hollow rectangle 	$S = \frac{BH^2}{6} - \frac{bh^3}{6H}$
I-Beam 	$S = \frac{BH^2}{6} - \frac{bh^3}{6H}$

Note: Adapted from “Section Modulus and Calculator Common Shape”, 2024, Engineers Edge.

In the final design concept, the rectangle was the chosen cross-section for the lower links of both legs. To provide a margin of safety, the final section moduluses were set at twice their minimum required. The chosen cross-sectional dimensions are displayed in Tables 7 & 8.

Table 7. Cross-sectional dimensions for front leg links

Leg Type	Cross Section Type	Dimensions (mm)	Section Modulus (mm ³)
Upper Link	Hollow rectangle	Inner base = 21.00 Inner height = 41.22 Outer base = 25.00 Outer height = 46.25	3.61e+03
Lower Link	Rectangle	Base = 10.00 Height = 12.00	3.75e+02

Table 8. Cross-sectional dimensions for hind leg links

Leg Type	Cross Section Type	Dimensions (mm)	Section Modulus (mm ³)
Upper Link	Hollow rectangle	Inner base = 18.00 Inner height = 24.00 Outer base = 24.00 Outer height = 30.00	1.87e+03
Middle Link	Rectangle	Base = 14.00 Height = 20.00	9.33
Lower Link	Rectangle	Base = 10.00 Height = 15.00	2.40e+02

Finite Element Analysis

A static structural finite element analysis (FEA) was conducted on each of the metal components using Ansys Workbench. The pinned connections and screw contacts were modelled as frictionless supports and a load equivalent to the robot's weight was applied in the direction of maximum bending, which is the direction perpendicular to the analyzed link. The elements were modelled as tetrahedrons with an element size of 0.5 mm. Mesh convergence was attempted to be implemented to obtain even more accurate results, however the element size could not be reduced any further due to limited RAM onboard the PC running the simulation, and therefore the element size was kept to the minimum possible 0.5 mm for the simulation.

Fig. 23 displays the results of the FEA static structural analysis. Comparing these FEA results to the shear moment diagrams presented in Fig. 23, it can be seen that the point of maximum bending moment corresponds to the approximate location of the maximum stresses in the FEA results, showing an agreement between the simplified 2D statics analysis and the FEA results.

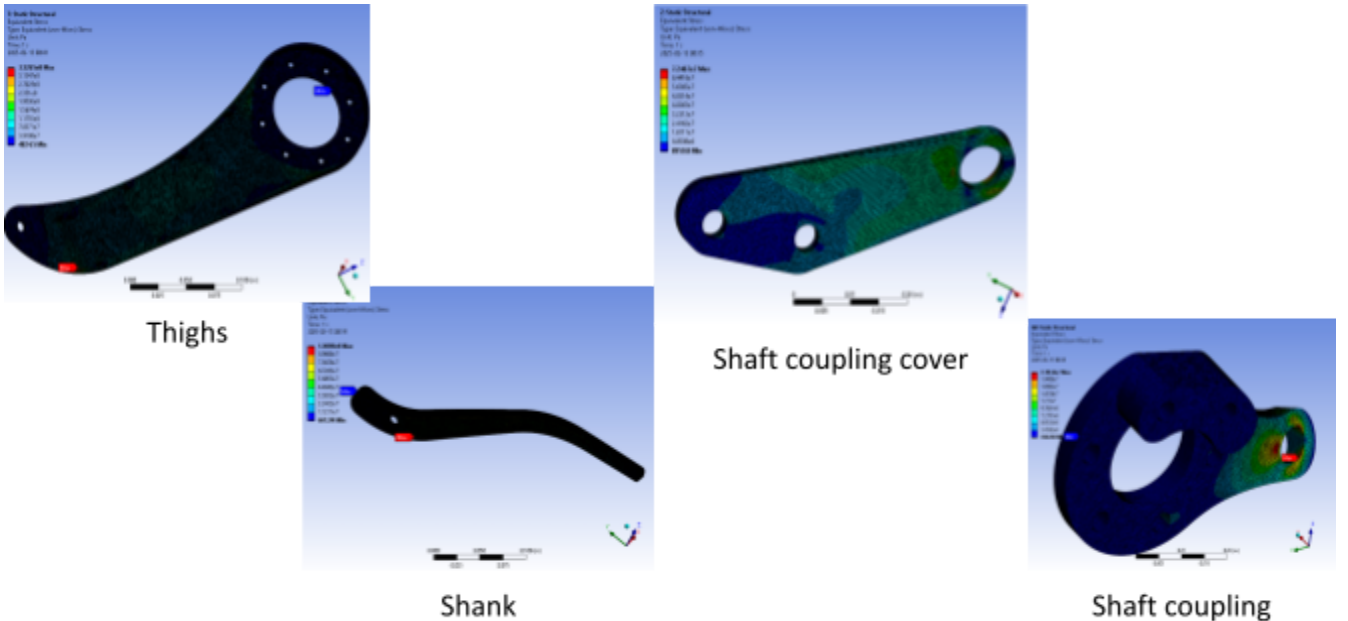


Figure 23. ANSYS analysis results

Buckling Analysis

By-hand buckling analysis was conducted to evaluate the stability under compressive loads, as listed in Fig. 24. Our sponsor required us to conduct buckling analysis of the lower links, which they stated is a common failure reason for legged robots. The Euler Column buckling formula is given by

$$F_{cr} = \frac{\pi^2 EI}{L_e} \quad (6)$$

where F_{cr} is the critical compressive buckling force, E is the elastic modulus, I is the moment of area, and L_e is the length of the member. Using the smallest area moment of inertia of $I = 2.812 \times 10^{-9} m^4$ derived from the section modulus of the lower link in Table 7, we calculated the P_{cr} to be 74,700 N, which exceeds the calculated impact force of 485.25 N. This ensures that the legs do not buckle, even under extreme conditions.

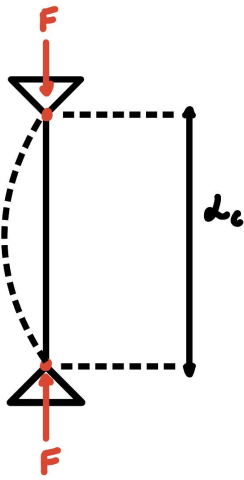


Figure 24. Euler Buckling Analysis Diagram

Impact Force Calculation

Our robot will be traveling on planes with its owners and will be treated as carry-on luggage at times, in particular on airplanes. The hardware design must be able to withstand a fall at that height. The maximum height was assumed to be the height from the floor of the aircraft to the overhead cabinet height (“How Are Overhead Bins Being Modified?”).

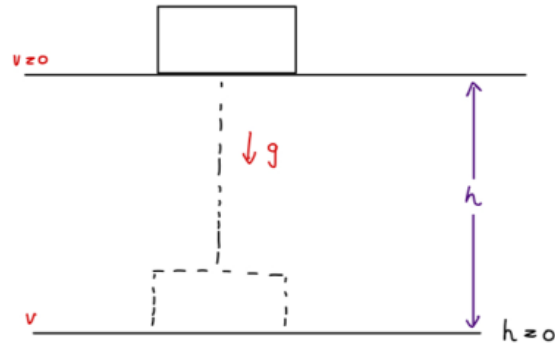


Figure 25. Diagram illustrating the free fall of the robot from the overhead cabinet of an aircraft.

Within the analysis, air resistance was neglected and using energy conservation between the floor of the aircraft and height of the cabinet,

$$\text{Total potential energy of the system} = \text{Total kinetic energy of the system}$$

$$\frac{1}{2}mv_0^2 + \frac{1}{2}mv_1^2 = mgh_0 + mgh_1 \quad (7)$$

where m is the mass of the robot, g is the gravitational acceleration, v_0 is the initial velocity, v_1 is the final velocity, h_0 is the initial height and h_1 is the final height.

Since $v_0 = 0$ and $h_1 = 0$, eq (7) is simplified to,

$$v_1 = \sqrt{2gh_0} \quad (8)$$

where $g = 9.81 \text{ m/s}^2$ and $h_0 = 2.1336 \text{ m}$ (84 inches) Therefore equation (8) gives v_1 (velocity when the object hits the ground) = 6.47 m/s. Using $F = ma$, to find the impact force at collision with the ground,

$$F = ma = \frac{m\Delta v}{\Delta t} = \frac{m(v_2 - v_1)}{\Delta t} \quad (9)$$

where F is the impact force, v_1 is the velocity when it hits the ground, v_2 is the velocity when it decelerates to stop after hitting the ground, and Δt is the time taken for the collision (time taken for the velocity to come to zero).

Assuming the time for a collision to be 200 ms, considering the mass to be 15 kg (mass of the robot) and $v_2 = 0$, from equation (9), we get the impact force to be, 485.25 N.

Since the impact force is smaller than the dynamic load of the robot, we considered the dynamic load to be the maximum force the robot will have to withstand.

Deflection and Strength Analysis of the Body:

The custom off-the-shelf metal frame of the body sustains all of the forces transmitted from the legs. To ensure adequate durability, the deflection and strength were analyzed. A load condition of 8.8 times the robot's weight was established, since we expect the maximum reaction force of the robot to be 2.2 times the robot's weight per leg, corresponding to a total load of 8.8 times the robot's

weight for the entire robot. This reaction force value is the exact number required for a slightly larger robot, the MIT Cheetah 3, generated at its peak torque (Bledt). The free body diagram of this analysis is shown in Fig. 26 and 27. It is to note that the cross section of the metal frame was assumed to be a U-channel, by combining the two angled brackets that go along the side of the body.

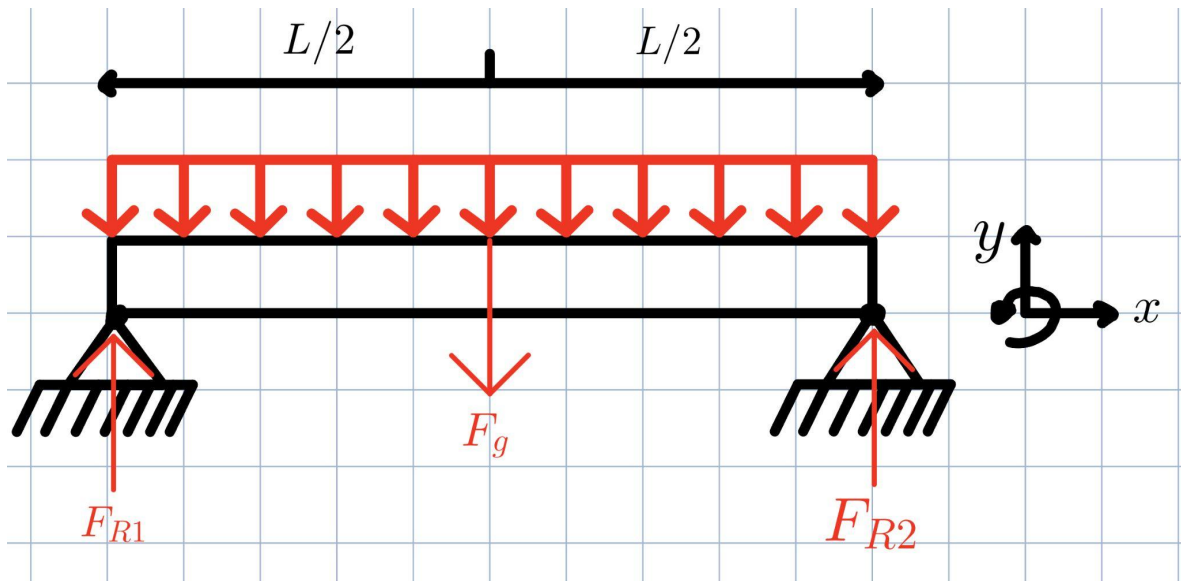


Figure 26. 2D Free Body Diagram of the Body

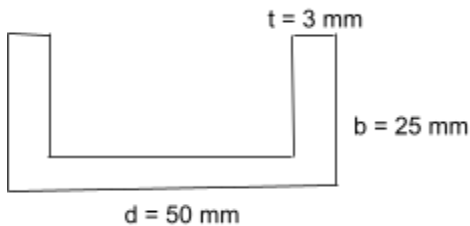


Figure 27. Cross section of body

During this analysis it was assumed the load was equally distributed across the entire body and equal to the total weight of the robot of about 19 kg. The following values were used: $E = 68 \text{ [GPa]}$, $L = 0.314 \text{ [mm]}$, $F_g = 8.8mg$, and $I = 1.64 \cdot 10^{-8} \text{ [m}^4]$. The modelled beam has simple supports at each end, mimicking the motor joints at each leg of the robot. The formula for the moment of inertia of this

cross section is shown in equation 10 (“Calculator Moment of Inertia, Section Modulus, Radii of Gyration Equations Channel Sections”) (“ASM Material Data Sheet”).

$$I = \frac{2tb^3 + (d-2t)t^3}{3} - (bd - (d - 2t)(b - t)) \frac{2b^2t + (d-2t)}{2bd - 2h(b-t)} \quad (10)$$

The formula for the maximum deflection from a distributed load in a simply supported beam is given by Juvinal (Juvinal):

$$\delta_{max} = \frac{5(\frac{F_g}{L})L^4}{384EI} = 0.06 \text{ [mm]} \quad (11)$$

In addition, the maximum moment resulting from the distributed load on a simply supported beam is given by Juvinal (Juvinal):

$$M_{max} = \frac{(F_g / L) * L^2}{8} = 64.7179 \text{ [Nm]} \quad (12)$$

Then, using equation 3, assuming $c = 25 \text{ [mm]}$, we obtain a maximum stress of $\sigma_{max} = 9.86 \text{ MPa}$. This is significantly under the yield strength of aluminum 6061 of 276 MPa (“ASM Material Data Sheet”), ensuring durability of the body under significant stress.

Kinematic Analysis

To validate the robot’s ability to climb stairs of standard height and optimize the link lengths to be as short as possible to maximize portability, an inverse kinematics analysis was conducted on each leg design using the stair climbing evaluation method developed by Barasuol et al (Barasuol). The code for this analysis is available in the GitHub repository listed in Appendix D. The inverse kinematics problem was formulated in 2D for four steps of stairs of standard height, in compliance with ADA standards (“Chapter 5: Stairways”).

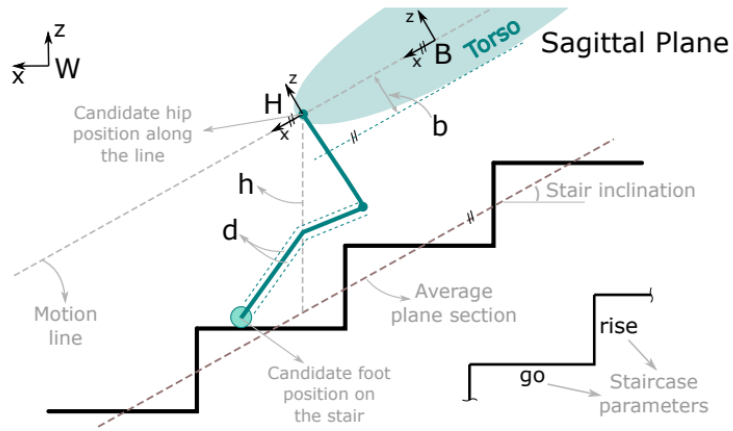


Figure 28. Stair climbing analysis, from work by Barasuol et al. (Barasuol)

In accordance to Barasuol et al's stair-climbing analysis, the following assumptions were made:

- Robot moves along the motion line
- Stair dimension of 7" x 11", under ADA standards ("Chapter 5: Stairways")
- Point foot is a circle
- Hip motor does not move (i.e. treat as 2 DoF planar kinematics problem)

Following the dimensions displayed in Figure 28, the adjustable parameters of the analysis are listed as follows:

Table 9. Stair Analysis Design Variables.

Parameter	Variable
Belly thickness	b
Body height	h
Link thickness	d
Go (stair length)	g
Rise (stair height)	r

To implement the stair climbing evaluation method, the forward kinematics were derived for each leg design, as shown in Figure 28, where the forward kinematics equations are represented as:

$$x = l_1 \cos(\theta_1) + l_2 \cos(\theta_1 + \theta_2) \quad (13)$$

$$y = l_1 \sin(\theta_1) + l_2 \sin(\theta_1 + \theta_2) \quad (14)$$

Using the forward kinematics equations, a Jacobian matrix in the world frame was derived for the inverse kinematics solver, where,

$$J = \begin{bmatrix} \frac{\partial x}{\partial \theta_1} & \frac{\partial x}{\partial \theta_2} \\ \frac{\partial y}{\partial \theta_1} & \frac{\partial y}{\partial \theta_2} \end{bmatrix} \quad (15)$$

The inverse kinematics for each leg was solved using the Newton-Raphson method to calculate the joint angles required to reach each desired footstep location (Anstee; Lynch and Park). The possible footstep locations were established by dividing the staircase by discrete points that are 1 cm apart.

The analysis is conducted as follows. Initially, the robot's dimension (belly thickness, link lengths, link thickness), are defined. Then, starting from a hip height set by the user, the inverse kinematics from the foot to each discrete point along the staircase. Any foothold position that causes the robot to reach its joint limit or penetrate the staircase are deemed as failure. Upon completion of the iterative inverse kinematics calculations of the initial hip position, the stair surface coverage, defined as the number of successful foothold positions / total number of discrete points, is calculated. A visualization of the foothold positions is shown in Figure 29.

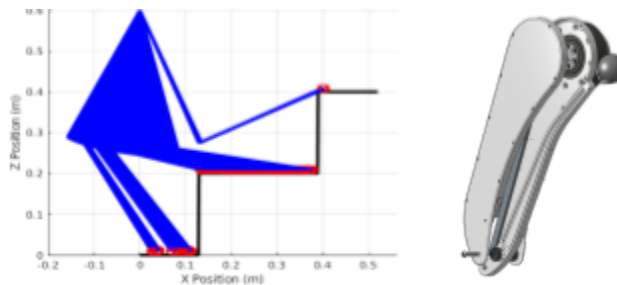


Figure 29. Kinematic visualization of legs at one hip height.

In Barasuol et al's work, leg designs capable of achieving 20% stair surface coverage were deemed to be successful at stair climbing. In our analysis, we increased this value to 30% to add a margin of safety. This increased staircase surface coverage requirement ensures that our robot has a larger workspace to promote stable stair climbing, which is crucial for a guide dog robot.

On top of validating the robot's ability to climb stairs, this analysis was used to shorten the links as much as possible to maximize portability while ensuring stair climbing. Minimization of the body height was also taken into consideration to maximize walking stability. Using a trial and error process, different combinations of link lengths and body heights were tested, arriving at a body height of 65 cm and link lengths Table 10 for the prototype design.

Table 10. Link lengths after optimization through stair climbing analysis.

	Leg Length (mm)
Upper Link	300 mm
Lower Link	330 mm

Dynamics Analysis

To ensure the robot is capable of generating sufficient ground reaction forces for both walking and stair climbing, a 2D inverse dynamics analysis was conducted to obtain the torque requirements of the actuators. By limiting the search space to within the expected joint angle ranges of the robot derived from the stair climbing analysis, the motor torques required to generate 75 N in the global Z direction (half of the robot's assumed weight) were calculated. The virtual work equation $\tau = J^T F_{tip}$ was utilized to find the motor torques, where $\tau \in \Re^{2 \times 1}$ is the vector of motor torques, $J \in \Re^{2 \times 2}$ is the Jacobian matrix in the world frame, and $F_{tip} \in \Re^{2 \times 1}$ is the reaction force applied at the foot in the global Z direction. This method ensures the actuators are properly sized to meet the mechanical requirements of the robot's locomotion tasks while optimizing performance within the expected operational range.

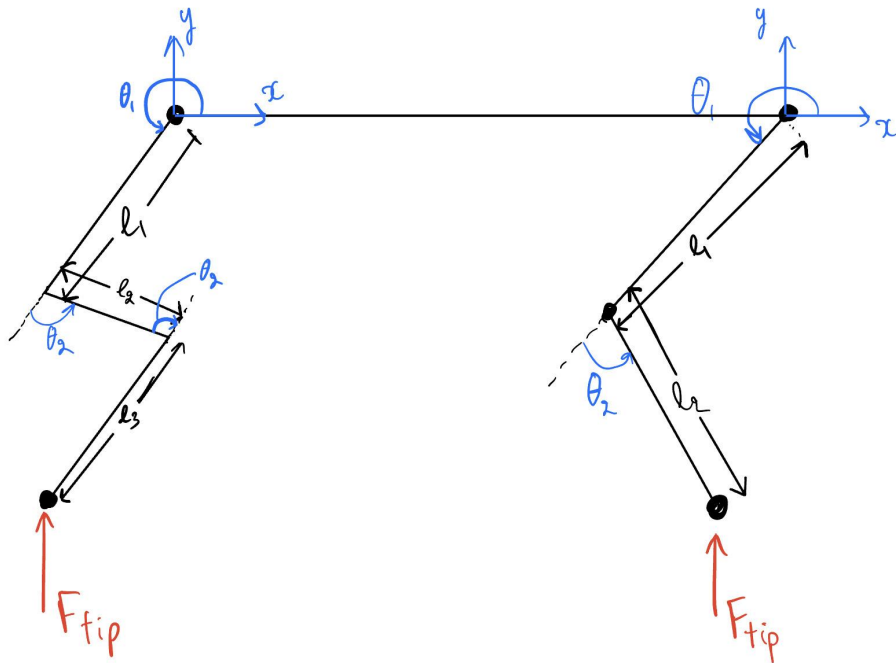


Figure 30. Free body diagram of inverse dynamics analysis, of old hind leg (left) and current leg design (right)

From the prototype of the CAD, the joint limit of the flexion/extension motor was found to be approximately (20° , 160°) for each leg. Using these values, the maximum torque values of 17 Nm and 14 Nm were obtained from all leg designs, for the flexion/extension and abduction/adduction actuators, respectively. To streamline motor control, we used the same motors for each type of joint. The chosen motor for all joints was the Unitree M8610 motor, which has a peak torque of 24 Nm. The selection of these motors was confirmed with our sponsor.

Final Design

The final design is presented in Fig. 31a. The two-link leg design is incorporated for all four legs. As shown in Fig. 31b, the robot is able to collapse to carry-on suitcase dimensions.

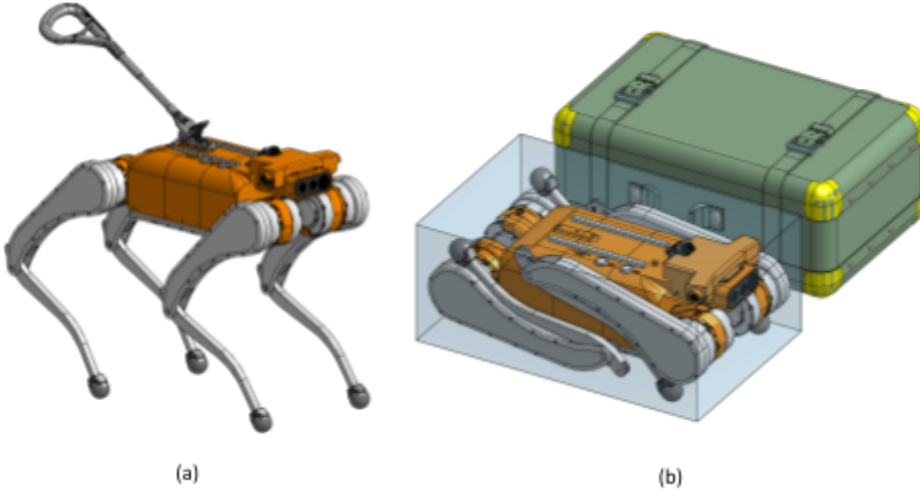


Figure 31. Final design concept. (a) Full robot assembly. (b) Comparison to carry-on suitcase size.

The body is constructed from a custom off-the-shelf metal frame and 3D printed covers. A rigid leash provided by the sponsor can be attached to the top cover. Additionally, screw rails along the length of the body allow for additional electronics to be mounted if the user desires to. The metal frame is designed to sustain all of the impacts transmitted through the legs, while the 3D printed components act as a mounting point for electronics. This two piece design allows for easy changes to the robot body design in the future, as our sponsor has easy access to 3D printing.

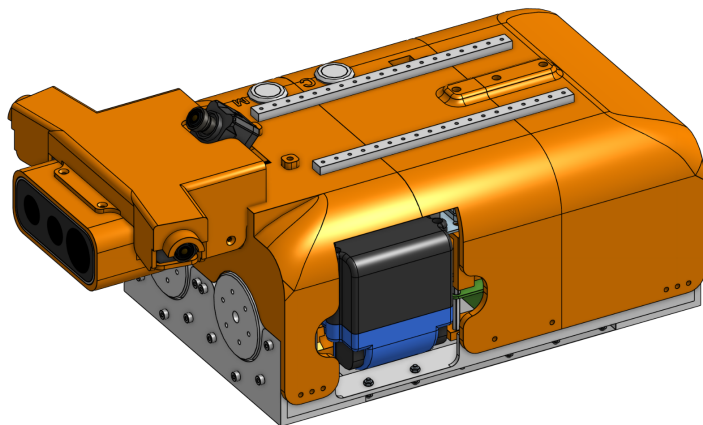


Figure 32. Isometric view of the body

The robot is powered by a single FLEX 24 V 12 Ah drill battery, which is designed to provide extended battery life. These batteries are both easily accessible and swappable, ensuring convenience and efficiency during operation.

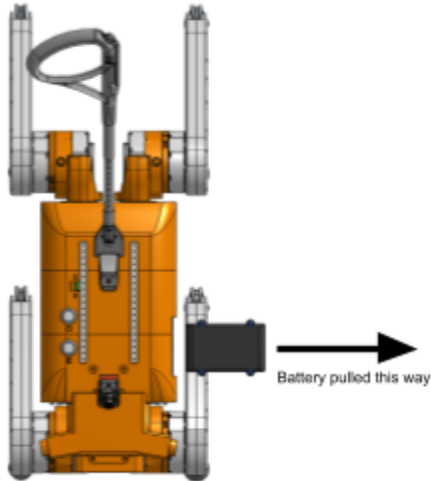
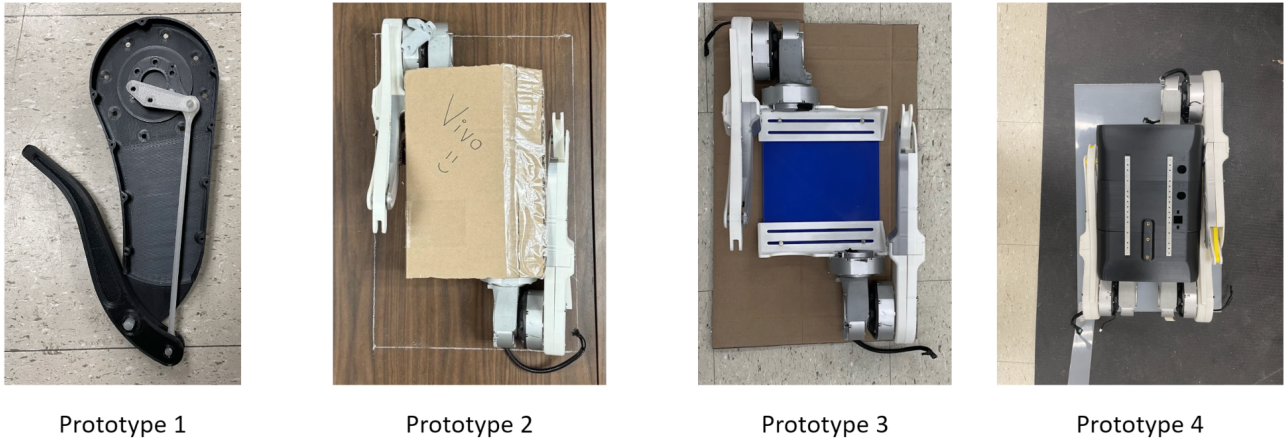


Figure 33. Body top view showing battery removal.

The final design of the legs feature three degrees of freedom. The stair climbing analysis and structural analyses ensure the legs are capable of stair climbing while able to withstand large loads (see “Statics Analysis” and “Kinematics Analysis” in Analysis section). All metal components are designed to be manufactured by 6-axis CNC milling.

Design Evaluation

An evaluation process was created to determine whether the robot meets the set specifications of mass, storage volume, and stair climbing. Several prototypes were made for evaluation and presentation purposes as seen in Fig. 34.



Prototype 1

Prototype 2

Prototype 3

Prototype 4

Figure 34. Prototypes for Evaluation and Presentation Purposes

In order to evaluate the mass (portability) of the robot the available components of prototype four (iteration prior to the final design) were measured in kilograms using a scale. For the unavailable electronic components such as the computers the respective data sheets were used, and for more complex parts such as the metal leg covers, the mass was estimated on Onshape using the approximate density and volume of the object.

It is important to note there will be a back camera mount in a further iteration of the design so six ZED cameras were included in the final mass calculation, though the camera mount mass was neglected since it has not been made. Based on previous designs from the lab the additional camera mount is estimated to weigh approximately the same as the front camera mount if not less (which would still meet the set specification). The body parts weight calculation (3.875 [kg], in Appendix D) is based on prototype four and does not account for the front part of the cover (red portion) with the new integrated camera mount. The camera mount design was instead added on separately before it was printed and meshed with the front cover (using Onshape), due to time constraints and more iterations and attention being necessary for this portion of the design. The final weight calculations (technically a mass measurement in kg) can be seen in Appendix D. The metal leg designs were also changed slightly to lower costs (added material), after prototype four. Using Onshape this additional mass was added on and the final weight was adjusted.

To evaluate storage volume (storability) of the robot each prototype (starting from prototype two) was tested to see if it could fit in carry-on suitcase dimensions via a ruler or tape measure, and a visual comparison such as the chalk box or plastic cutout seen in Fig. 34. When the prototypes failed to meet specifications, it was noted, and future iterations were adjusted accordingly like the motor placement previously discussed.

The final portion of the evaluation was related to stair climbing. This section of the evaluation was split into simple leg joint movement tests, and a dynamic simulation. A smaller version of the leg (prototype one in Fig. 34), was used to evaluate whether the mechanism responsible for stair climbing actually works using a 3D-printed crank in place of the motor in order to drive the shank. Later in the process full scale 3D-printed legs were tested using a reachability test. A cardboard staircase was created for this test measured and cut to the dimensions of the rise/go specifications. The leg was moved by hand to see if it could move smoothly and could reach the desired stair height (Fig. 43). After this prior to knowing the dynamic simulation would be complete in time for the showcase a stop motion video of the final robot design was made demonstrating that the legs could go through the approximate motions necessary for stair climbing (Fig. 44). The body had to be held up, and the legs had to be moved by hand because the 3D-prints would not be able to withstand the weight of the body or torques acted upon them. Motor control was removed from our scope. The final portion was a dynamic simulation (Fig. 45). A URDF file was set up with necessary joint limits and similar specifications for our design and a graduate student conducted a simulation designed to teach the robot how to walk (machine learning).

Evaluation Results

Portability Testing

The portability test was a success with the final mass coming out to be 19.1 [kg] which is less than the 21.5 [kg] ideal value.



Figure 35. Scale Pictures

Storability Testing

Prototype two was made in order to test the storability of the design. It was created with 3D-printed legs and a cardboard box. The cardboard box was made to represent the max body size needed based on the CAD to fit all the electronics needed by the sponsor. Brackets were also created to hold the motors up to their correct positions (Fig. 36). Some adjustments were made to

accommodate bigger motors in the new second semester body design which was still in progress (radius of the new motors added on to each side of the body). This prototype was compared to carry-on suitcase dimensions via direct comparison (chalk box) and using a ruler. The prototype ended up being too long lengthwise, being slightly out of specification (Fig. 37).

Based on this failure, the required distance between the motors was taken into account for the next iteration of the design and prototype three was created to represent this new body length. Prototype three was found as seen in Fig. 38 to fit within constraints (the cardboard it is laying on is the carry-on length and width specification). Prototype four with a more finalized design as seen in Fig. 39 also fit within the body dimension constraints coming in at: $53.97 \times 28.58 \times 17.15 \text{ cm}^3$ which was less than $55.88 \times 35.56 \times 22.86 \text{ cm}^3$ along all lengths. The final design was also tested via comparison of the carry-on suitcase dimensions and also fits within the constraint (Fig. 39 and 40).



Figure 36. Bracket design for prototype two and three

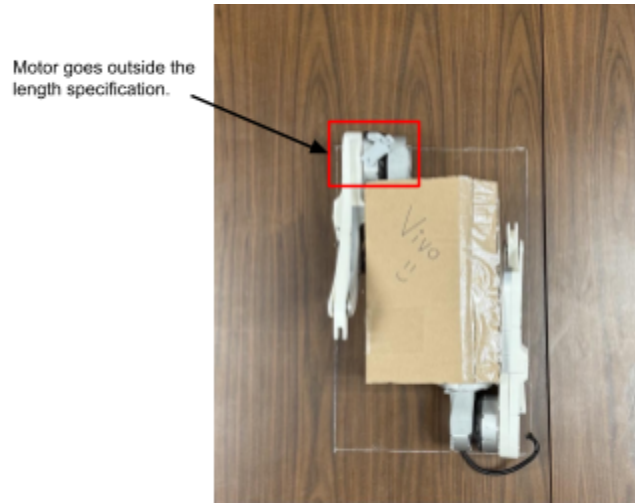


Figure 37. Prototype 2 storability test (fail)



Figure 38. Prototype 3 storability test (pass)



Figure 39. Prototype 4 storability test (pass)

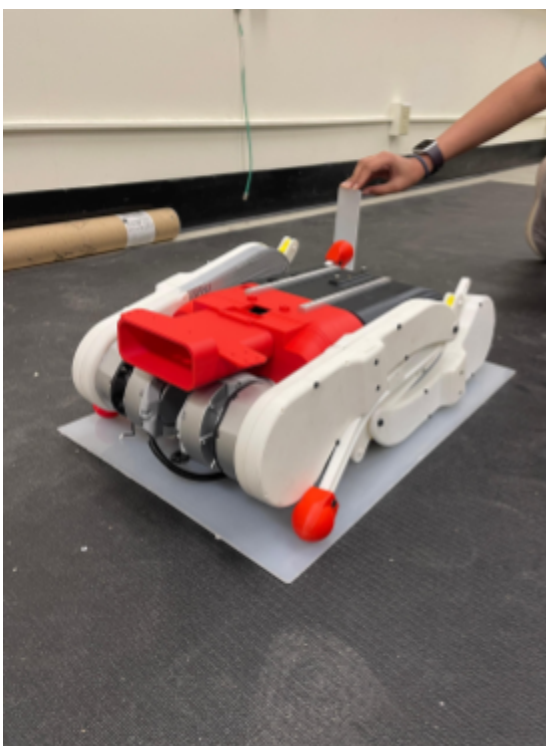


Figure 40. Final design test (Pass)

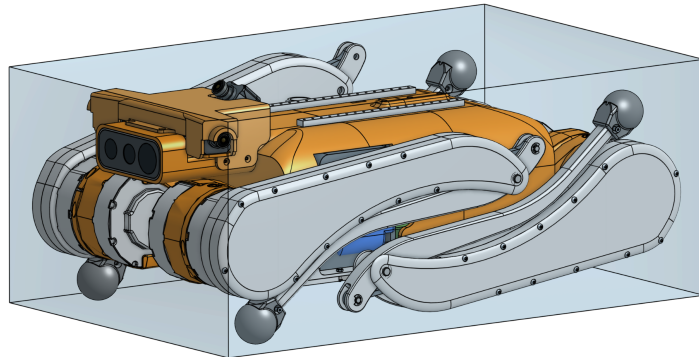


Figure 41. Vivo fits within Carry-on Dimensions (final design in CAD)

Stair Climbing Tests:

The leg joint movement tests were both successful via visual inspection. The small leg (prototype 1) moved smoothly when the crank was moved (Fig. 42). The larger 3D printed legs during the reachability test had similar results (Fig. 43), and the foot was able to reach up and touch the top of the cardboard stair based on our rise/go specifications. Both these tests had successful results. The stop-motion video demonstrating the approximate motions necessary for stair climbing was also successful and was able to show visually that the leg could go through the motions and still reach the ideal staircase dimensions (Fig. 44). The final dynamic simulation (though still in the early stages of machine learning), output (which is a video or moving model in the workspace) clear results that the robot would have the capability to climb our set stair rise and go (Fig. 45).



Figure 42. Prototype 1 leg joint movement test

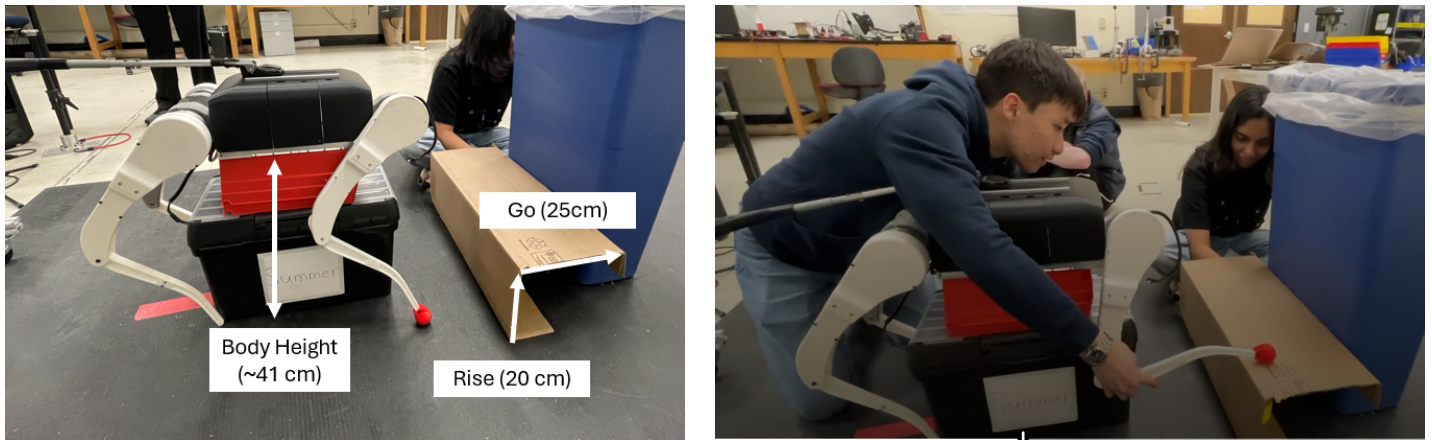


Figure 43. Prototype four reachability test

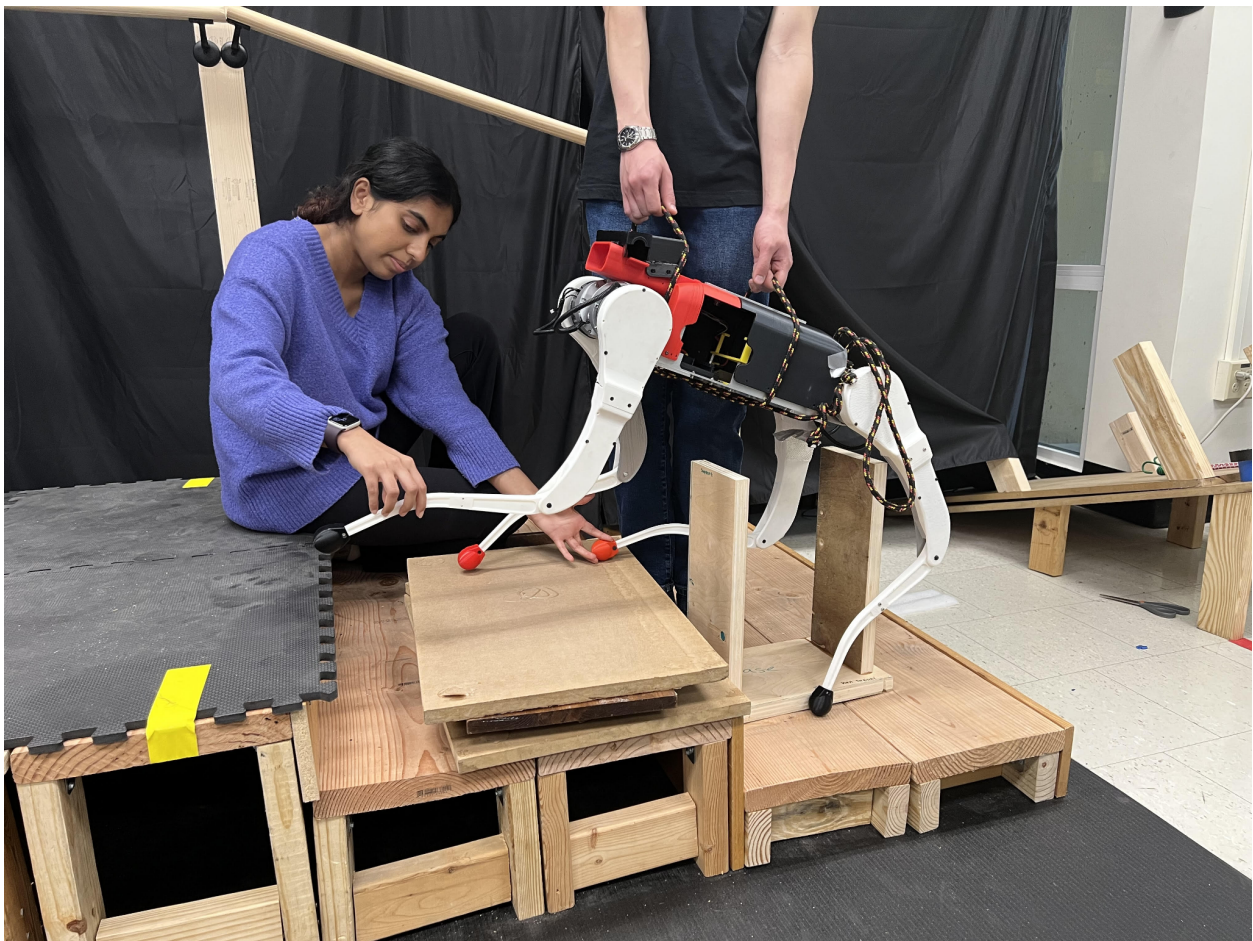


Figure 44. Final prototype portion of stop-motion video

Two examples of the dog being able to climb stairs.

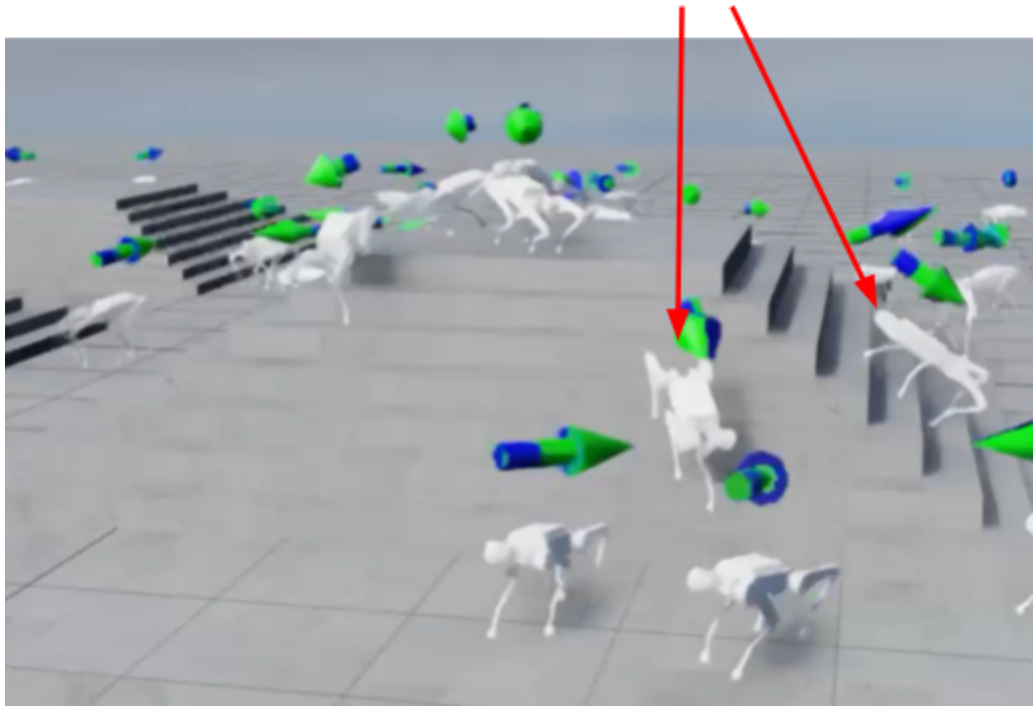


Figure 45. Dynamic simulation output

Conclusions and Recommendations

Vivo was created to provide our sponsor with a specialized research platform to facilitate further the research and development of the vision algorithms, path planning, and controller design required to mimic the functionality of a guide dog. In this sense, our team and sponsor have deemed this project a success. While logistics issues outside of the team's control prevented assembly of the final metal legs, the sponsor is prepared to complete these final steps with the help of a team member. More effort must be put into establishing motor control before controllers can be tested. Future iterations of this prototype should optimize the body design because it is the sub-assembly with the most room for improvement since the design was changed to account for uncertain budgetary constraints.

Integrative Experience

Guide dogs are used by many BLV users but they typically come with heavy associated costs, high responsibility, a limited timespan before retiring, and limited availability. The robot guide dog offers an excellent solution to these commonly overlooked problems that are a struggle for many BLV individuals. Our design cuts the cost of owning a guide dog in half and allows for future iterations. Though this project mainly aims to create a quadruped robot for lab research purposes, it is likely future iterations would lead to mass-production which would address not only guide dog availability but the common financial concerns and burdens that follow.

The dog was designed with the user's needs first, which has required additional research into common guide dog interactions and necessities beyond the scope of the typical engineering curriculum. Designing the legs of the robot required research into the anatomy of dogs and advanced robotics. The daily life of a BLV user was also taken into account when designing our robot. The hind legs were designed with the ability for the user to brush their leg up against the robot, as is commonplace with traditional guide dogs. When BLV users go about their daily lives, they often need to take public transportation (Hwang). For this purpose, the dog was designed to be able to fit in a suitcase form factor and its battery life was increased from the sponsor's current robot. This project has gone beyond just a standard engineering design process to not simply make a barebones prototype for future iterations, but one that already addresses critical real-world problems with the current design. This project has pushed the team to think beyond just engineering and to think in the perspective of a BLV user.

This project was a collaborative effort for the entire group. In order to design and fabricate a robot all members of the group had to be involved in every aspect of the project. This project helped grow each team member's ability to work in a group. Team members' opinions were respected and heard and constructive criticism was given and received. Many group members were able to take risks and design and fabricate new parts. Working in a group taught team members to play off people's strengths and expect mistakes to occur. Overall this project allowed for group work at a high level, comparable to real-world projects.

Presenting our work in different ways has been an important part of this project. The team has presented in front of many different audiences such as professors, students, industry professionals, etc. The team has learned to understand the perspective of the audience and understand the different levels of knowledge for the material. Tailoring our discussions to the audience allows us to inform others in a way best suited for them. Due to time constraints, the team has learned to choose which pieces of information are most important for the audience's understanding. Written reports have given us the opportunity to explain in greater detail all aspects of the project, such as our preliminary research and our engineering analyses.

References

Al Zavier, Maried. "Exploring the Use of a Drone to Guide Blind Runners." *ASSETS '16: Proceedings of the 18th International ACM SIGACCESS Conference on Computers and Accessibility*, 2016, pp. 263-264, <https://dl.acm.org/doi/abs/10.1145/2982142.2982204>.

Anstee, Richard. "The Newton-Raphson Method." *Department of Mathematics, The University of British Columbia*, The University of British Columbia,
<https://personal.math.ubc.ca/~anstee/math104/newtonmethod.pdf>.

"ASM Material Data Sheet." *ASM Material Data Sheet*,
<https://asm.matweb.com/search/specificmaterial.asp?bassnum=ma6061t6>. Accessed 8 November 2024.

Barasuol, Victor. "Stair-Climbing Charts: On the Optimal Body Height for Quadruped Robots to Walk on Stairs." *Synergetic Cooperation Between Robots and Humans: Proceedings of the CLAWAR 2023 Conference—Volume 1*, Springer Nature Switzerland, 2024. Accessed 8 November 2024.

Bledt, Gerardo. "MIT Cheetah 3: Design and Control of a Robust, Dynamic Quadruped Robot." *IEEE International Conference on Intelligent Robots and Systems*, 2019. *MIT Libraries*,
<https://hdl.handle.net/1721.1/126619>.

"Calculator Moment of Inertia, Section Modulus, Radii of Gyration Equations Channel Sections." *Engineers Edge*,
https://www.engineersedge.com/material_science/moment-inertia-gyration-5.htm#.

"Chapter 5: Stairways." *Access Board*,
<https://www.access-board.gov/ada/guides/chapter-5-stairways/>. Accessed 5 December 2024.

“Copper, Cu; Annealed.” *MatWeb*,

<https://www.matweb.com/search/DataSheet.aspx?MatGUID=9aebe83845c04c1db5126fada6f76f7e&ckck=1>.

De Vicenti, Flavio. “Control-Aware Design Optimization for Bio-Inspired Quadruped Robots.” 2021 *IEEE/RSJ International Conference on Intelligent Robots and Systems (IROS). International Institute of Electrical Engineers (IEEE)*, <https://ieeexplore.ieee.org/document/9636415>.

Durant, A. M. “Kinematics of stair ascent in healthy dogs.” *Veterinary and Comparative Orthopaedics and Traumatology*, 2011,

https://www.researchgate.net/publication/49763291_Kinematics_of_stair_ascent_in_healthy_dogs.

Guerreiro, João. “CaBot: Designing and Evaluating an Autonomous Navigation Robot for Blind People.” *ASSETS '19: Proceedings of the 21st International ACM SIGACCESS Conference on Computers and Accessibility*, 2019, pp. 68-82, <https://dl.acm.org/doi/abs/10.1145/3308561.3353771>.

“Guide Dog Class Lectures: Working in Buildings.” *Guide Dogs for the Blind*,
<https://www.guidedogs.com/resources/client-resources/guide-dog-class-lecture-materials/working-in-buildings>. Accessed 8 November 2024.

“How Are Overhead Bins Being Modified?” *Rosen Aviation*, 21 February 2024,
<https://www.rosenaviation.com/blog/how-are-overhead-bins-being-modified/>. Accessed 8 November 2024.

“How Much Does A Guide Dog Cost?” *Puppy In Training*, 17 September 2017,
<https://puppyintraining.com/how-much-does-a-guide-dog-cost/>.

Hwang, Hochul. "Towards Robotic Companions: Understanding Handler-Guide Dog Interactions for Informed Guide Dog Robot Design." *CHI '24: Proceedings of the 2024 CHI Conference on Human Factors in Computing Systems*, 2024, pp. 1-20, <https://doi.org/10.1145/3613904.3642181>.

"Industrial Inspection Solutions." *Boston Dynamics*, <https://bostondynamics.com/solutions/inspection/>. Accessed 8 November 2024.

Juvinal, Robert C., and Kurt M. Marshek. *Fundamentals of Machine Component Design*. Wiley, 2019.

Katz, Benjamin G. "A low cost modular actuator for dynamic robots." *Massachusetts Institute of Technology*, 2018, <http://hdl.handle.net/1721.1/118671>.

Layosa, Carlicia. *Timing Belt Failure and Maintenance | MISUMI Mech Lab Blog*, 15 January 2016, <https://us.misumi-ec.com/blog/timing-belt-maintenance-and-belt-failure/>. Accessed 9 November 2024.

Lee, Jongwoo. "Energy-efficient robotic leg design using redundantly actuated parallel mechanism." *2017 IEEE International Conference on Advanced Intelligent Mechatronics (AIM). International Institute of Electrical Engineers (IEEE)*, <https://ieeexplore.ieee.org/document/8014182>.

Lynch, Kevin M., and Frank C. Park. *Modern Robotics: Mechanics, Planning, and Control*. Cambridge University Press, 2017.

Museum of Veterinary Anatomy FMVZ USP. *Golden Retriever dog. Canis lupus familiaris*. English: Specimen of golden retriever skeleton prepared by the bone maceration technique and on display at the Museum of Veterinary Anatomy, FMVZ USP. 2016. *Wikimedia Commons*, https://commons.wikimedia.org/wiki/File:Golden_Retriever_dog_at_MAV-USP.jpg.

Norcross, Amanda. "Carry-on Luggage Size and Weight Limits by Airline (2024)." *U.S. News Travel*,

<https://travel.usnews.com/features/carry-on-luggage-sizes-size-restrictions-by-airline>.

Accessed 8 November 2024.

Park, Hae-Won. "High-speed bounding with the MIT Cheetah 2: Control design and experiments." *The International Journal of Robotics Research*, vol. 36, no. 2, 2017. *MIT Libraries*,

<http://hdl.handle.net/1721.1/119686>. Accessed November 2024.

Piper, Grant. "10 Guide Dog Breeds: Info, Pictures, Facts, & Traits." *Hepper Blog*, 2024,

<https://www.hepper.com/guide-dog-breeds/>.

Potter, Steve D. *Screw Actuator for a Legged Robot*. US20220003297A1. United States Patent and

Trademark Office, <https://patents.google.com/patent/US20220003297A1/en>.

RegulusRemains. *Unitree Go1 Calf Actuator*.

<https://youtube.com/shorts/KVS0Xwg15Tc?si=qpyzFfFymUei5XW5>.

"SAE 1018 Steel – Chemical Composition, Material, Properties and Uses." *Solitaire Overseas*,

<https://www.solitaire-overseas.com/blog/sae-1018-steel-composition-properties/>. Accessed 8

November 2024.

Scafato, Alessandro Schiavone. *Limb portion of robot*. WO2022207106A1. The United States Patent

and Trademark Office, 2021, <https://patents.google.com/patent/WO2022207106A1/>.

Seok, Sangok. "Design Principles for Energy-Efficient Legged Locomotion and Implementation on the

MIT Cheetah Robot." *IEEE/ASME Transactions on Mechatronics* 20.3 (2015), 2014, p. 1117,

<http://dx.doi.org/10.1109/TMECH.2014.2339013>.

Slade, Patrick. "Multimodal sensing and intuitive steering assistance improve navigation and mobility for people with impaired vision." *Science Robotics*, vol. 6, no. 59, 2021,
<https://www.science.org/doi/full/10.1126/scirobotics.abg6594>.

Standard Specification for Aluminum-Alloy 6061-T6 Standard Structural Profiles. American Society for Testing and Materials, 2010.

Tachi, Susumu. "Guide Dog Robot." *Mechanical Engineering Laboratory, Ministry of International Trade and Industry*, 1985, <https://files.tachilab.org/publications/paper1900/tachi1985MIT.pdf>.

"Thermoplastics - Physical Properties." *The Engineering ToolBox*,
https://www.engineeringtoolbox.com/physical-properties-thermoplastics-d_808.html.
Accessed 8 November 2024.

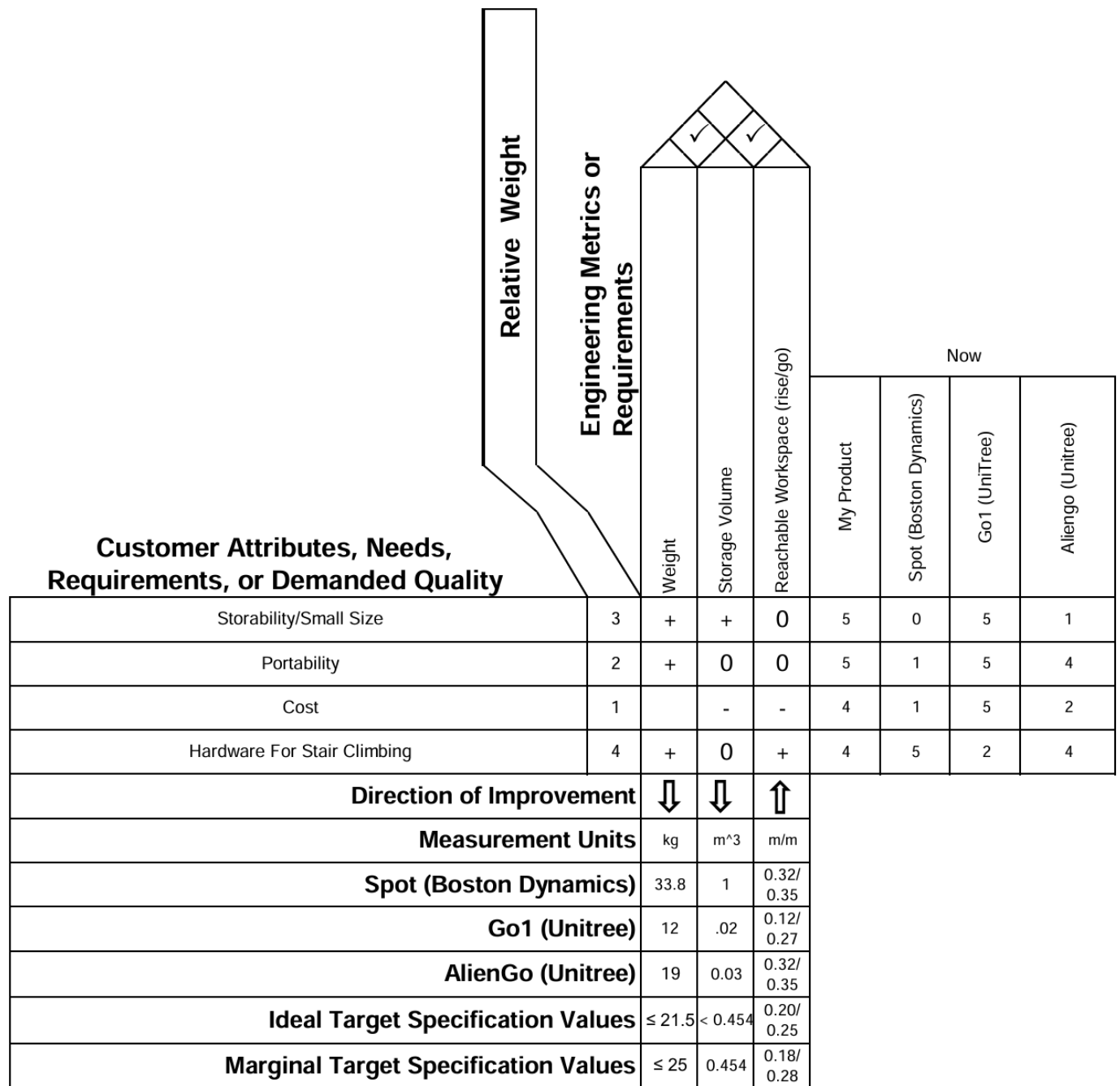
"Unitree Go1." *Unitree*, <https://www.unitree.com/go1>.

APPENDIX A: Bill of Materials for Prototype

Count	Stock No.	Item Name	URL	Unit Price (USD)	Total Price (USD)	Supplier	Comments
4	298-20182-ND	Panduit Corp PMV6-3R-L	https://www.digikey.com/en/products/detail/panduit/298-20182-nd/100	\$1.37	\$5.48	DigiKey	For crimping battery connections
6	1217558-2-ND	TE Connectivity AMP Connectors 1217558-2	https://www.digikey.com/en/products/detail/te-connectivity/1217558-2/100	\$0.28	\$1.68	DigiKey	Battery terminals
4	298-16737-ND	Panduit Corp ESV8-ESV10-Q	https://www.digikey.com/en/products/detail/panduit/298-16737-nd/100	\$5.06	\$20.24	DigiKey	For crimping connections to anti spark switch
6	298-9996-ND	Panduit Corp BSV10X-D	https://www.digikey.com/en/products/detail/panduit/298-9996-nd/100	\$0.62	\$3.72	DigiKey	For crimping connections to anti spark switch
2	B0BX2Q5C6J	Flipsky Anti Spark Switch Aluminum PCB 90V 300A for Electric Skateboard/Ebik/e/Scooter/Robots	https://www.amazon.com	\$39.99	\$79.98	Amazon	Anti spark switch
1	B08L3RS5HP	3 Pairs Amass XT90H XT90 Wire XT 90 Plug Male and Female Connector 150mm 10AWG Silicon Wire for RC Lipo Battery FPV Racing Drone	https://www.amazon.com	\$11.99	\$11.99	Amazon	Power supply line for motor power distribution board
1	B07C5KJX24	8 Pairs XT30 Plug Male Female Connector with 150mm 16AWG Silicone Wire for RC LiPo Battery FPV Drone	https://www.amazon.com	\$12.99	\$12.99	Amazon	Power supply line for motor power distribution board to motors
1	B072BXB2Y8	(Real 18AWG) 10 Pairs 12V 5A DC Power Pigtail Barrel Plug Connector Cable, 2.1mm x 5.5mm Male Female DC Pigtail Connectors for CCTV Security Camera and 12V Power Supply Adapter by MILAPEAK	https://www.amazon.com	\$9.49	\$9.49	Amazon	Power supply lines for computers and ethernet switch

		NETGEAR 5-Port Gigabit Ethernet Easy Smart Managed Essentials Switch (GS305E) - Desktop or Wall Mount, Home Network Hub, Office Ethernet Splitter, Silent Operation	https://www.amazon.com/NETGEAR-GS305E-5-Port-Gigabit-Ethernet/dp/B07PJ7XZ7X	\$19.99	\$19.99	Amazon	Ethernet switch
1	B07VBJ2HRC	Cat 6 Ethernet Network Cable RJ45 Male to Female Shielded Ethernet Network Connector Screw Panel Mount Extension Cable for Router, Modem (0.3M/1ft)	https://www.amazon.com/Cat-Ethernet-Extender-Router-Modem/dp/B07VBJ2HRC	\$6.99	\$6.99	Amazon	Ethernet extender
1		Displayport 1.4 Male to Female Extension Cable DP to DP Extended Cord with Screws Panel Mount 4k/60hz 2K@144Hz Supports Audio&Video for Monitor TV PC Laptop 1.6ft/0.5m	https://www.amazon.com/Displayport-Male-Female-Extension-Cable/dp/B07WVQH9LJ	\$9.99	\$9.99	Amazon	
1	96741A114	Brass Pan Head Phillips Screws, M3 x 0.5 mm Thread, 5 mm Long	https://www.mcmaster.com/96741A114	\$12.73	\$12.73	McMaster-Carr	For screwing in battery terminals
1	92095A216	Button Head M5x0.8 x 25	https://www.mcmaster.com/92095A216	\$7.64	\$7.64	McMaster	
1	92010A799	Flat Head Countersink M3.5x0.6 x 8	https://www.mcmaster.com/92010A799	\$3.63	\$3.63	McMaster	
1	91274A115	Socket Head M4x0.7 x 8	https://www.mcmaster.com/91274A115	\$5.28	\$5.28	McMaster	
1	94500A266	Button Head M3x0.5 x 20	https://www.mcmaster.com/94500A266	\$7.73	\$7.73	McMaster	
BOM #2							
Quantity (Per Leg)				Cost Per Piece			
<u>Needle Roller Be</u>				\$28.36	MISUMI		
<u>Deep Groove Be</u>				\$12.94	MISUMI		
<u>Precision Pivot F</u>				\$17.08	MISUMI		
<u>Precision Pivot F</u>				\$29.44	MISUMI		
<u>Precision Pivot F</u>				\$30.66	MISUMI		
Total: \$338.03							
*Note this does not include the price of the legs and is only for things bought off the MIE budget.							

APPENDIX B: House of Quality



APPENDIX C: Stair Climbing Analysis & Inverse Dynamics Code Repositories

[Stair Climbing Analysis Script](#)

[Inverse Dynamics Analysis Scripts](#)

APPENDIX D: Evaluation Weight Calculations

$$\text{Final Weight} = W_{\text{body components}} + W_{\text{motors}} + W_{\text{TPU Feet}} + W_{\text{metal legs}} + W_{\text{Six ZED Cameras}} + W_{\text{Azure Connect Camera}} + W_{\text{computers}} + W_{\text{front camera mount}}$$

$$\text{Weight of motor} = W_{\text{3D printed leg w/motor}} - W_{\text{3D printed leg}}$$

$$\text{Final Weight} = 3.875 \text{ [kg]} + 6.940 \text{ [kg]} + 0.054 \text{ [kg]} + 6.060 \text{ [kg]} + 0.200 \text{ [kg]} + 0.400 \text{ [kg]} + 1.283 \text{ [kg]} + 0.271 \text{ [kg]} = \mathbf{19.083 \text{ [kg]}} \leq \mathbf{21.5 \text{ [kg]}}$$

Weight of body components: 3.875 [kg]

Weight of 3D-printed leg: 0.265 [kg] (scale)

Weight of motor: 1.735 [kg] (scale)

Estimated weight of metal leg: 1.515 [kg] (Onshape)

TPU Foot: 0.014 [kg] (scale)

ZED Camera: 0.050 [kg] (datasheet)

Azure Connect DK Camera: 0.440 [kg] (datasheet)

UpXtreme 114: 0.410 [kg] (scale)

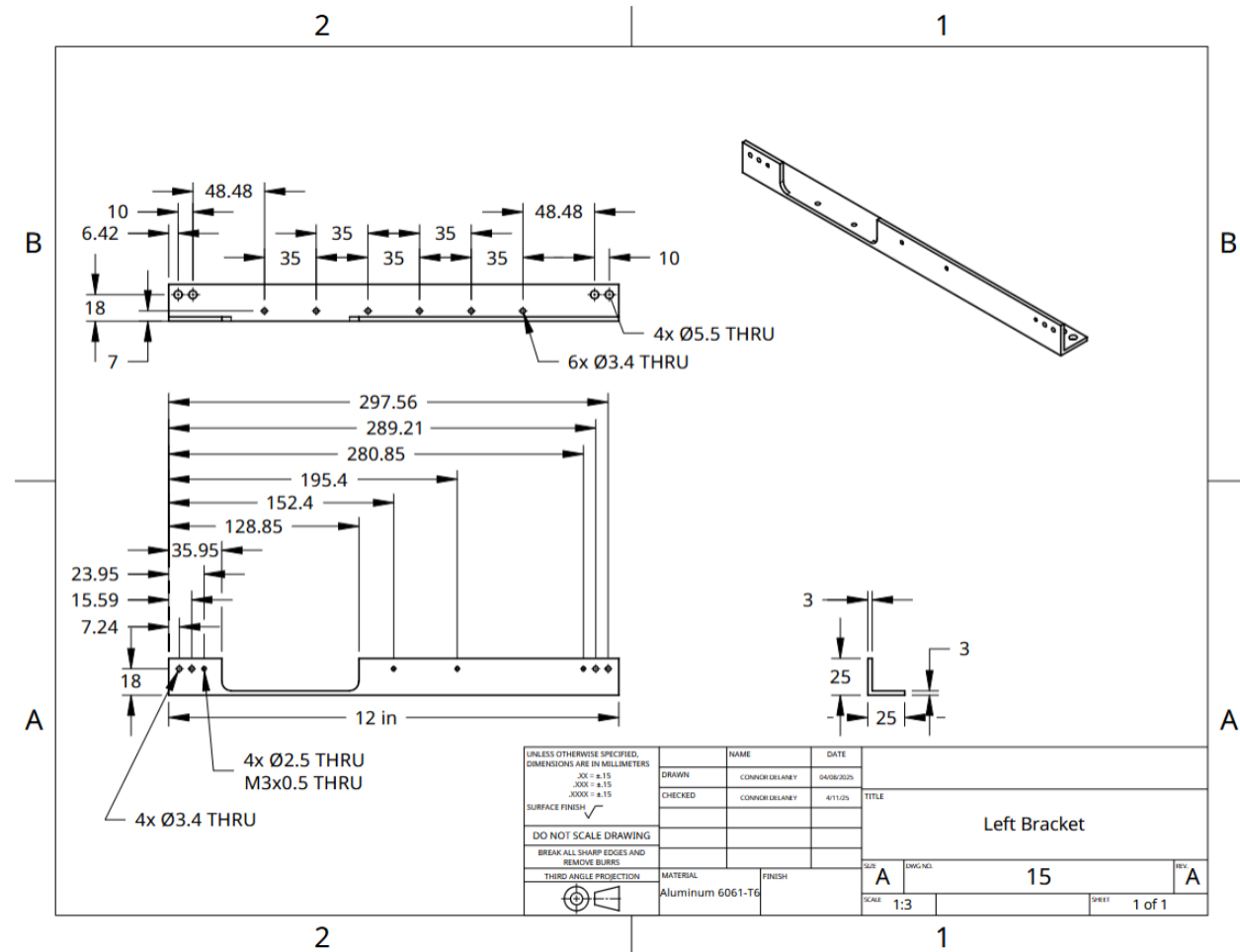
Orion Computer: 0.873 [kg] (datasheet)

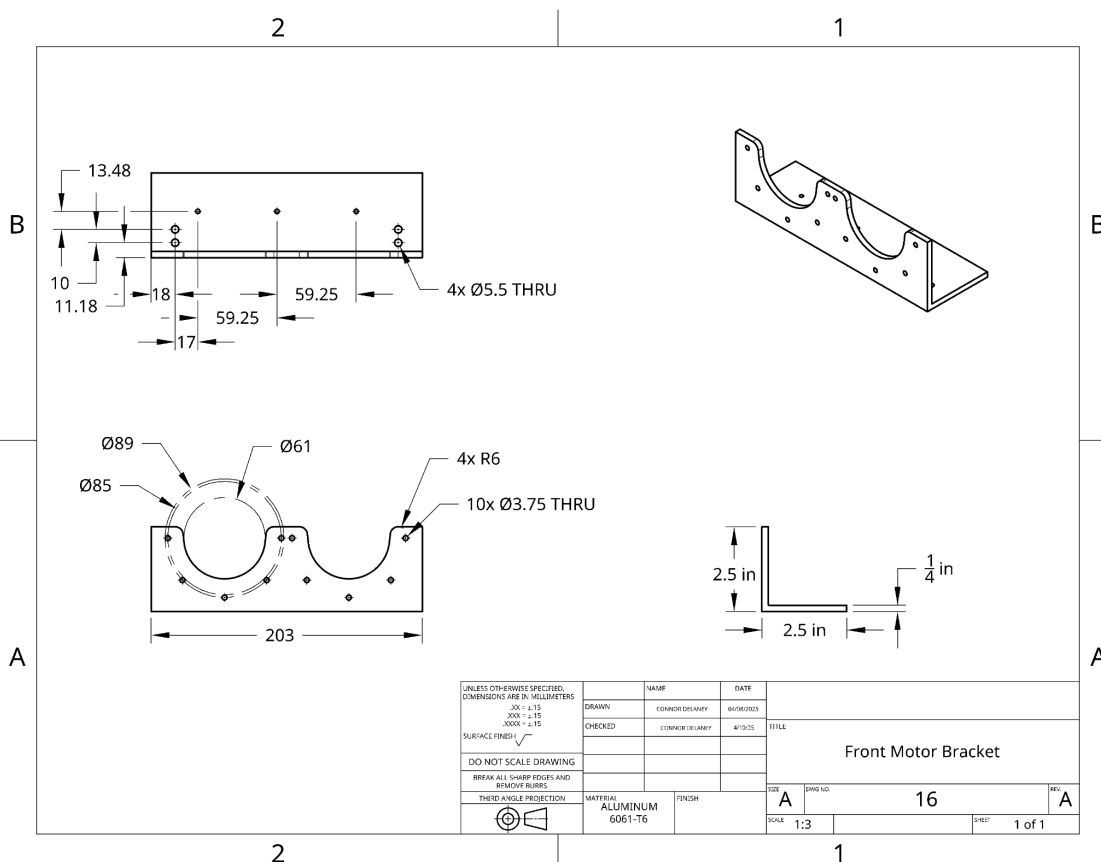
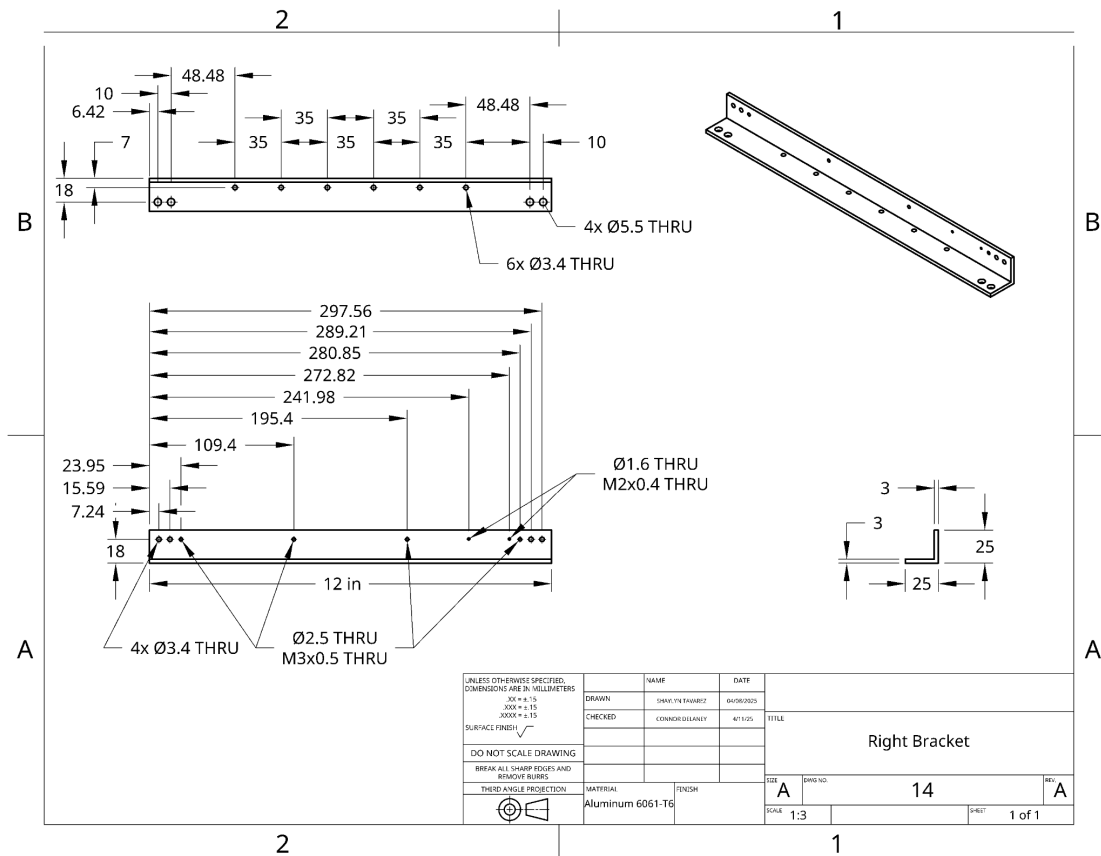
Weight of Front Camera Mount: 0.271 [kg] (Onshape)

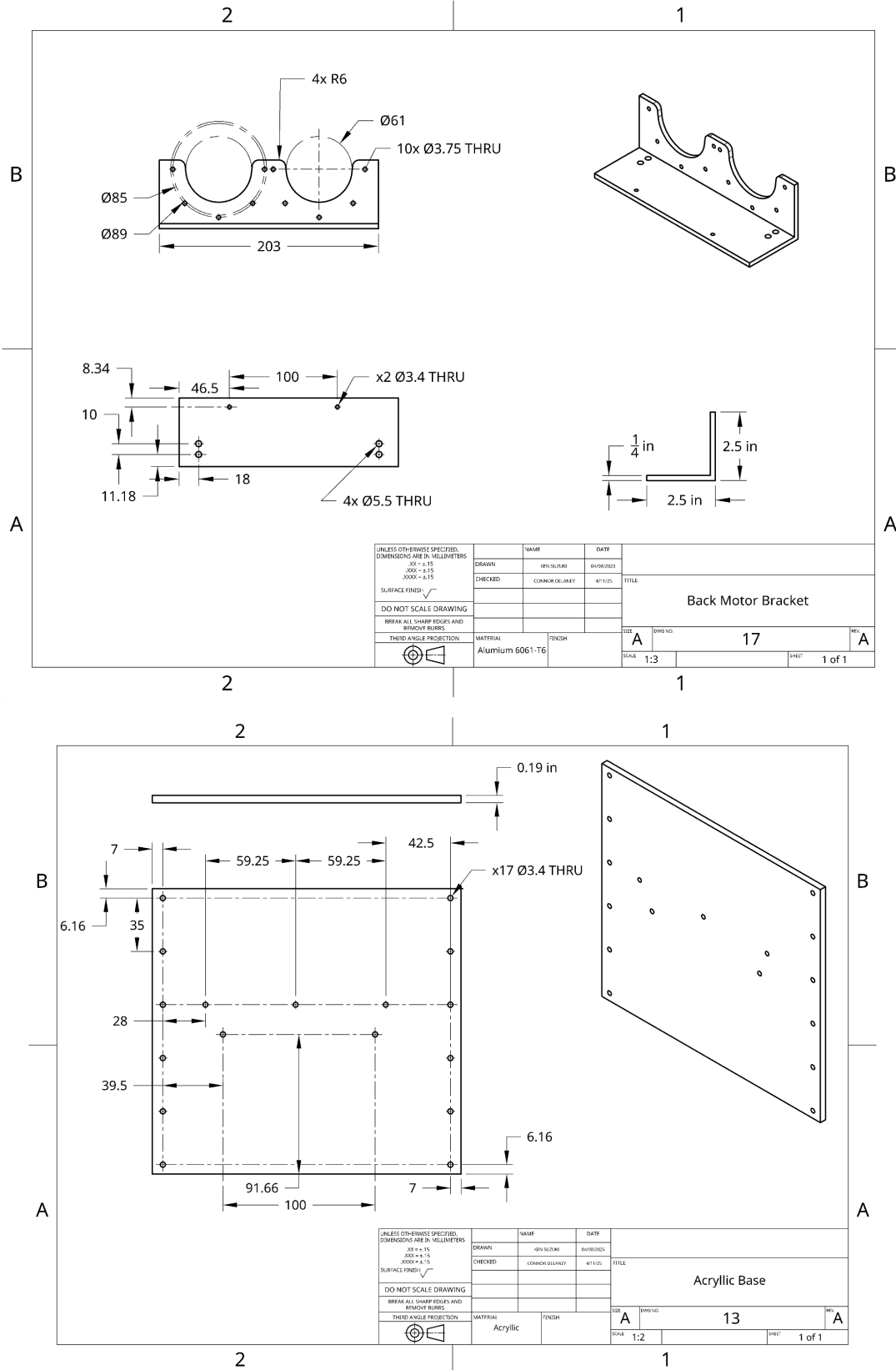
Calculation Notes:

- Back camera mount weight was neglected since it will be added in the future, and is expected to be approximately the same weight of the front camera mount or less. This estimate is based on previous robot dog camera mount designs and the front design including a bigger camera.
- Weight of body components does not include the computers, those were added on separately.

APPENDIX E: Additional Manufacturing Drawings







Drawings for contract manufacturer (also has access to CAD):

